The importance of Atlantic Water pathways for understanding glacier discharge in Northwest Greenland

Marije van Hell

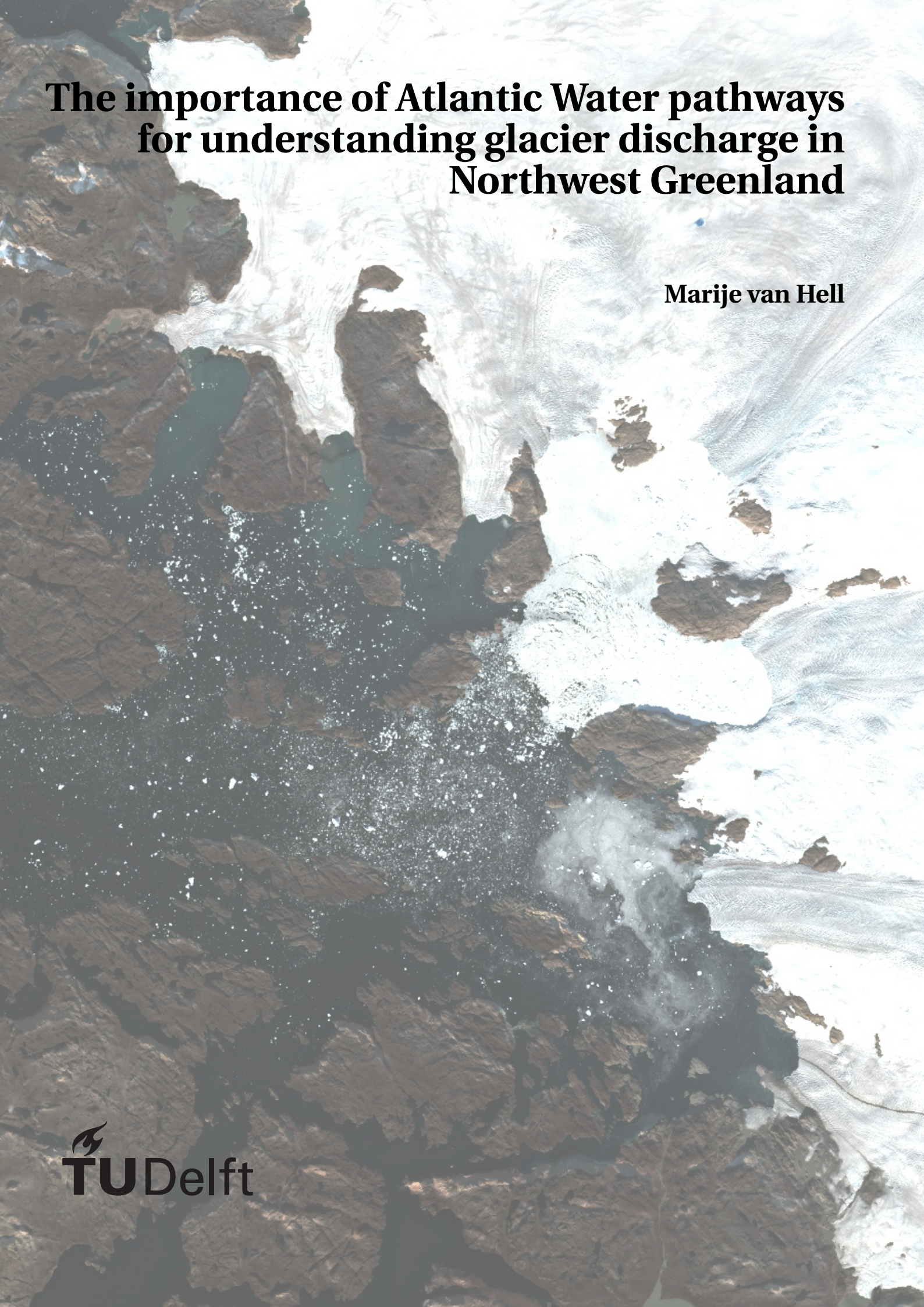

TU Delft

The importance of Atlantic Water pathways in understanding glacier discharge in Northwest Greenland

by

Marije van Hell

to obtain the degree of Master of Science
at the Delft University of Technology,
to be defended publicly on Monday January 17, 2022 at 15:00.

Student number: 4377915
Thesis committee: Dr. S. L. M. Lhermitte, TU Delft
Prof. Dr. J. D. Pietrzak, TU Delft
Dr. M. Vizcaino, TU Delft

The cover image shows a true color image of the Upernavik calving fronts obtained by the Sentinel-2 satellite in the summer of 2020.

TU Delft

Abstract

It is well known that warming of deep Atlantic Water in recent decades resulted in extensive retreat of marine terminating glaciers in Northwest Greenland and increased their discharge, which contributed significantly to sea level rise. Here we use data and model resources over a wide range of space and timescales to determine how the pathways of deep Atlantic Water, through the complex bathymetry of Melville Bay, increased the vulnerability of glaciers over the observed ocean warming period. New observations of salinity and temperature of the ocean water and bathymetry from NASA's Ocean Melting Greenland mission as well as Mankoff's discharge estimates are combined with FESOM and HYCOM ocean model results. We have shown that these pathways of Atlantic Water are crucial for understanding the increase in discharge of certain glaciers over the ocean warming period. More specifically, the vulnerability of a marine terminating glacier in Northwest Greenland to Atlantic Water depends on its latitudinal position, the location of the fjordal channel entrance along the Southern or Northern canyon head and whether the fjordal channel is deep enough to be a pathway for Baffin Bay Intermediate Water. The Upernavik N and C glaciers, which are in the most vulnerable position, contributed 10% to the total discharge change of Northwest Greenland. In addition, the glaciers that exhibited the largest normalised discharge change showed correspondence between their discharge estimates and the observed changes in fjord geometry during the retreat of the glacier calving front. Warming of deep Atlantic Water impacted the normalised discharge estimates, but the sensitivity of the fjord geometry also controlled large parts of the observed trends. With this study, new insights in the vulnerability of marine terminating glaciers were obtained, which showed that the pathways of Atlantic Water should not be overlooked when developing climate models.

Preface

The beauty of the extensive availability of open data sources, is the opportunity to study areas that you might never visit in real life, but that are still very important to processes on Earth. In my case, Northwest Greenland. I am very happy that I could combine my passion for snow, ice and water into one final project.

I would also like to take this opportunity to thank my supervisors. First of all, a big thanks to Stef, your advise always steered me in the right direction and your sharp eye was a very big support in translating my explanations during our meetings into the right visualisations. Without you, my figures would not have been as descriptive as they are now. Julie, I have always enjoyed our meetings where we discussed everything ocean, especially when we could finally do them in real life again. I learned a lot from you, and I am extremely grateful for the big amount of time you spend with me in the end to help me get my thoughts on paper in the right way. And finally, thank you Miren, your sharp observations during my green light meeting brought my thesis to the next level. I also want to say thanks to Claudia, who provided the FESOM model results to me and was always available over Skype to explain the model and discuss my findings.

Finally, I want to say thanks to my family and friends for listening to me babbling on and on about the subject to try and organise my thoughts. Special thanks to Emma, for the mental support and practically proof reading my whole thesis. Hannah, who picked me up and supported when it was really needed. Milou, Gup and Joos, for making the times in the TU Delft library a lot more enjoyable. Hein, Heleen, Luce and Loek for helping me move, during the most stressful period of my thesis and Fleur for the numerous days of coding and writing together with good coffee and lunch and many more great friends that were a welcome distraction over the past year.

So here it is, the thesis that marks the end of my time at TU Delft.

Enjoy reading!

Marije van Hell
Amsterdam, Monday 10^{th} of January, 2022

Contents

1 Introduction

The Greenland Ice Sheet contributes significantly to sea level rise and 32% can be traced back to the Northwest of Greenland for the period between 1972 and 2018 (Mouginot et al. 2019). In the same region, the largest glacier retreat (28% of the total) occurred from 1992 to 2017 (Wood et al. 2021). Northwest Greenland is controlled by changes in ice dynamics, it is the only region where discharge has increased (from 90 to 112 Gt/yr), while the Surface Mass Balance (SMB) has decreased (from 78 to 45 Gt/yr) between the periods 1972-1980 and 2010-2018 (Mouginot et al. 2019).

Since most of Northwest Greenland's glaciers are marine terminating (E. Rignot et al. 2015), they are affected by increasing temperatures of deep Atlantic Water. The warmer temperatures cause increased ocean-induced melting and faster retreat of glaciers (Khazendar et al. 2019; Wood et al. 2018). When a glacier retreats, it can become unstable, which in turn can increase discharge. King et al. (2020) have shown that Greenland Ice Sheet wide increases in discharge are mostly due to the retreat of calving fronts. The retreat pattern varies significantly from glacier to glacier, yet oceanic and atmospheric forcings varied little with latitude (Murray et al. 2015). However, the retreat has been connected to warming of Atlantic Waters (Wood et al. 2018).

Ocean currents play a key role in providing warmer deep Atlantic Water to the glaciers. These currents are driven by a clockwise circulation around Greenland that highlights the boundary current system that circulates around the Ice Sheet, from Fram Strait to Nares Sound (Fenty et al. 2016). This boundary current includes the East Greenland Current (EGC), Irminger Current (IC) and West Greenland Current (WGC) (Figure 1.1). The WGC transports water northward into Baffin Bay, the shelf portion consists of fresher waters from the East Greenland Current (Rudels et al. 2002) and the slope portion of warmer, saltier waters (Myers, Donnelly, and Ribergaard 2009). Near the coast river plumes transport meltwater from the numerous glaciers resulting in a clockwise coastal transport around Greenland. The resulting pathways are summarised in Figure 1.1.

Different water masses have different ocean temperature and salinity ranges, therefore it is key to discriminate the presence of the two dominant water masses in Baffin Bay; the Atlantic and Arctic Ocean water masses (Tang et al. 2004; Fenty et al. 2016). The Arctic water mass consists of fresh water of Arctic origin. It enters Baffin Bay from two locations, through Nares Strait, Jones and Lancaster Sounds forming the southward Baffin Island Current (Tang et al. 2004) and through the shelf portion of the WGC which transports fresher waters from the East Greenland Current northward (Rudels et al. 2002).

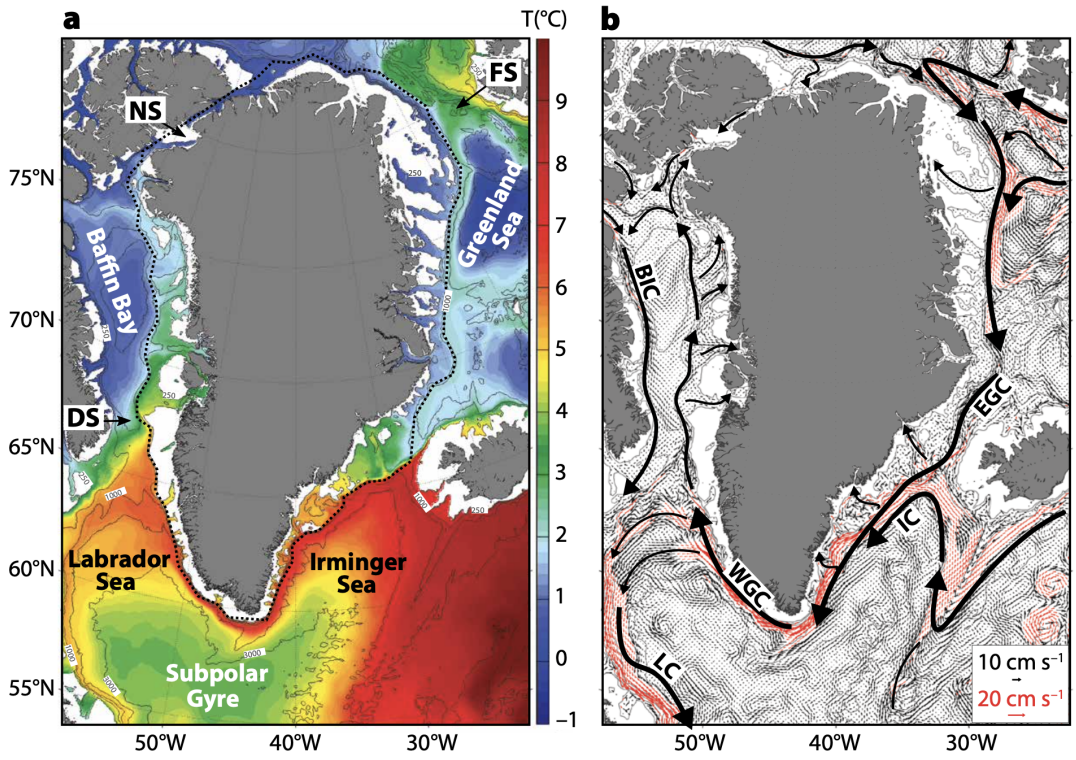

Figure 1.1: **Pathways of Atlantic originating and Arctic waters to Baffin Bay. Figure 1 from Fenty et al. (2016).** **(a)** 250 m depth ocean temperatures from a simulation of the MITgcm ocean circulation model. The dotted line indicates the boundary of the Greenland shelf. This line approximately corresponds to the 1000 m depth contour. Fram Strait (FS), Davis Strait (DS) and Nares Strait (NS) locations are also shown. **(b)** 250 m depth annual ocean velocity from the same MITgcm simulation illustrating the boundary currents around the Greenland shelf: West Greenland Current (WGC), Irminger Current(IC), Baffin Island Current (BIC), and Labrador Current (LC).

The Atlantic Water consists of warm, salty water that is denser and originates in the subtropics. The Atlantic Water is cooled and modified to Irminger Water in the Irminger Sea (Tang et al. 2004). Subsequently, the slope part of the WGC transports the Irminger water to the West coast of Greenland, where it mixes with Labrador Sea Water resulting in Modified Irminger Water (ModIrW). This flows northward through the East side of Davis Strait into Baffin Bay (Cuny, Rhines, and Kwok 2005; Curry et al. 2014; Tang et al. 2004). In Baffin Bay, cyclonic (counter-clockwise) ocean circulation cools the Atlantic originating waters as they circulate (Tang et al. 2004), forming Baffin Bay Intermediate Water (BBIntW) (Gladish, Holland, and Lee 2015). Grivault, Hu, and Myers (2017) found that the circulation is driven by a baroclinic gradient. During the process another water mass is formed, the mixing of Arctic and Atlantic originating waters creates Baffin Bay Thermal Water (BBTherW) (Gladish, Holland, and Lee 2015).

Each water mass that is present in Baffin Bay has a distinctive range of temperature and salinity. Figure 1.2a shows the vertical distribution of water masses in a section across Davis Strait. Figure 1.2b shows the different water masses as colored contours. Gladish, Holland, and Lee (2015) refer to Arctic Water as Baffin Bay Arctic Water (BBArcW). Baffin Bay Arctic water is the coldest least dense layer found just below the surface. Underneath the BBArcW, the Baffin Bay Thermal Water is present. This is a thin layer of water with a strong thermal gradient. It represents the thermocline between the BBArcW and BBIntW (Gladish, Holland, and Lee 2015). The BBIntW is the Atlantic originating water mass found from 300 to 800 m depth (Tang et al. 2004). In the deepest parts of Baffin Bay, dense and colder Baffin Bay Deep Water (BBDeepW) is present (Gladish, Holland, and Lee 2015).

Since the position of water masses in a water column depends on their density, the heavier warm BBIntW sits below the lighter colder BBArcW and BBTherW (Figure 1.1a). The potential density anomaly, displayed by the isopycnals in Figure 1.1b, of Baffin Bay Intermediate Water ranges from 27.4 to 27.675 g/kg. BBIntW is thus heavier than the Baffin Bay Arctic Water, which ranges from 26.0 to 27.0 g/kg and Baffin Bay Thermal Water, which reaches from 27.0 to 27.4 g/kg. The surface of the ocean is filled with light shelf waters with highly varying temperatures, visualised in black in Figure 1.1b.

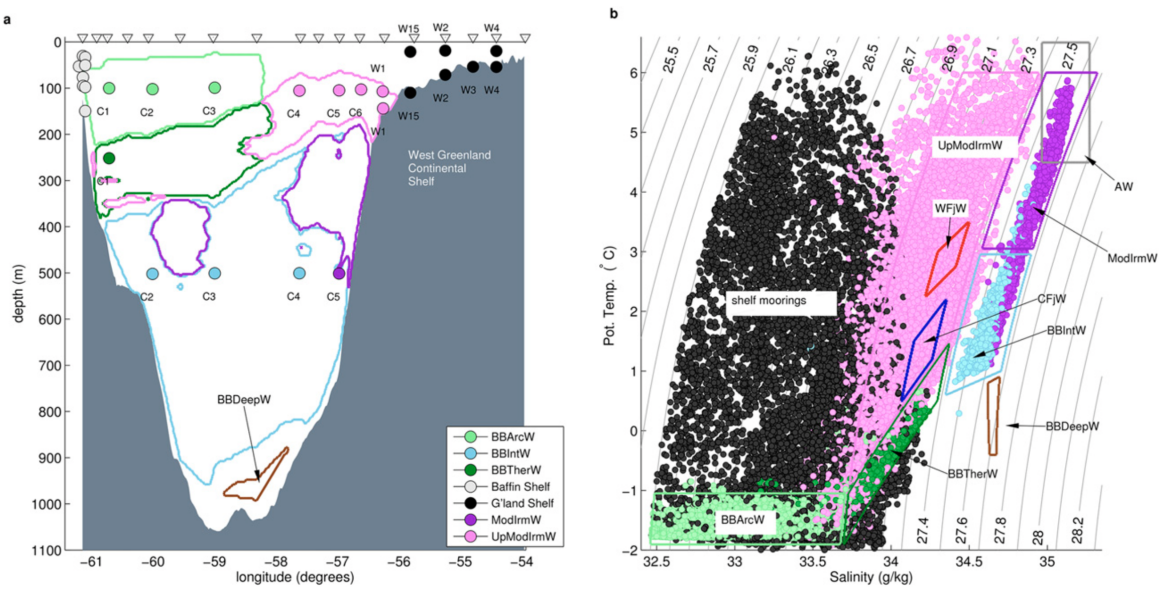

Figure 1.2: **Water masses in Davis Strait, cross section and potential temperature and absolute salinity diagram. Figure 2 from Gladish, Holland, and Lee (2015).** **(a)** Cross section of Davis Strait. The colored lines indicate the spatial distribution of water masses obtained from the Conductivity Temperature Depth (CTD) section of September 2004 along the Davis Strait mooring line. The stations where the CTD's were taken are marked by triangles. Locations of moorings, in depth and longitude, are indicated by circular markers. The moorings were in use between 2004 and 2011 and are in colored groups according to their similarity of water properties and spatial proximity. **(b)** Potential temperature (θ) and absolute salinity (SA) diagram that indicates the different water masses that exist in Davis Strait and Baffin Bay in colored contours that correspond to the colored lines in (a): BBArcW (Baffin Bay Arctic Water), BBTherW (Baffin Bay Thermal Water), BBIntW (Baffin Bay Intermediate Water), BBDeepW (Baffin Bay Deep Water) ModIrmW (Modified Irminger Water), UpModIrmW (Upper-Modified Irminger Water), AW (Atlantic Water). Warm Fjord Water (WFjW) and Cold Fjord Water (CFjW) are also shown in the diagram but not relevant for this study. The mooring observations are colored according to the legend in (a).The grey lines represent the lines of constant potential density (isopycnals) with reference to 1000 kg/m^3, referred to as potential density anomaly (σ_θ).

Canyons play a key role in the access of deep Atlantic Water currents to the glaciers. The bathymetry in central and Southwest Greenland is characterised by isolated, broad deep canyons (Figure 1.3a). The Northwest contrast starkly to the central and Southwest and is more complex (Morlighem et al. 2017). Two cross-shelf canyons incise the outer shelf of Northwest Greenland, which connect the open ocean to the inner shelfbreak (An et al. 2019). These pronounced features are up to 250 km long and 100 km wide and will be referred to as the Northern and Southern canyon (Figure 1.3b). The inner shelf fjordal channels are 5 to 10 km wide and 400 to 1200 m deep (An et al. 2019). From Upernavik S to Hayes N NN (Figure 1.3b) fjordal channels are deep, wide and connected. Northward from Hayes N NN, channels are less well developed (An et al. 2019).

Ocean topography is known to steer water masses. A frictionless, geostrophic flow follows the contours of the Coriolis force over depth (f/H). When the depth of the ocean bed decreases, the Coriolis force has to decrease. As a result, flow will be deflected towards the equator. At the location of cross shelf canyons, the flow can become ageostrophic. The Rossby number ($Ro = U/fL$, where U is the horizontal velocity scale, f the Coriolis parameter and L the horizontal length scale) increases as the characteristic length scale decreases from the shelf to the canyon width. Consequently, the effect of pressure gradients are now more important than the effect of the Coriolis force, resulting in upwelling or downwelling (Allen and Durrieu De Madron 2009). Upwelling in canyons is thought to increase the melting of the 79°N glacier (Münchow, Schaffer, and Kanzow 2020).

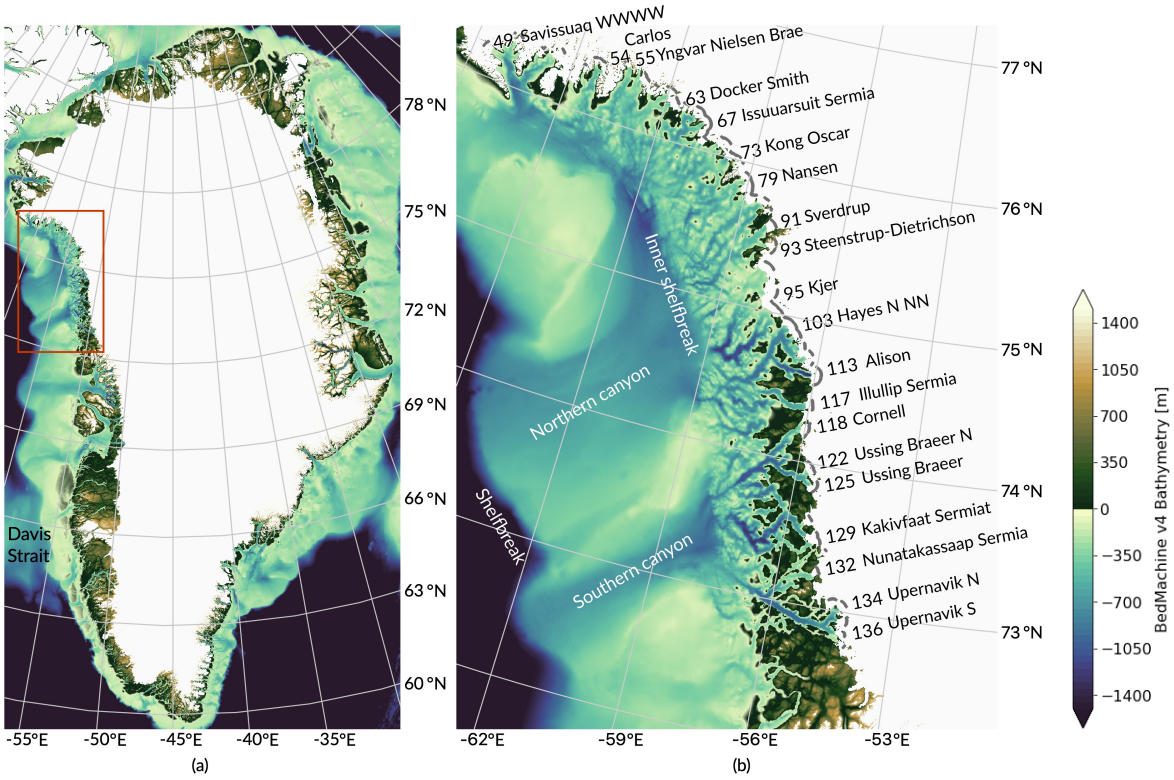

Figure 1.3: **Area of Interest: Northwest Greenland (Melville Bay). (a)** Overview map of Greenland. Bathymetry and ice mask from BedMachine v4 (Morlighem 2021; Morlighem et al. 2017). Red box indicates our area of interest Northwest Greenland. **(b)** Bathymetry of Northwest Greenland indicating the *Northern canyon* at 74°N, the *Southern canyon* at 73°N (light blue). The *real shelfbreak* located offshore in the west (dark blue), a second break in topography that we refer to as the *inner shelfbreak*, that is located to the Southwest of the *fjordal network system*. Glacier gate numbers and names of most marine terminating glaciers are shown, full list can be found in Appendix D

Moreover, the Baffin Bay Intermediate Water started warming in the mid-1990's (Wood et al. 2021). At that time the North Atlantic Oscillation (NOA) changed from a positive to a negative phase (Rignot et al. 2012; Sarafanov 2009), which caused the spreading of heat from the North Atlantic subpolar gyre. Subsequently, the heat flux through the Irminger and West Greenland Current was enhanced (Wood et al. 2021). Since 2010, the NAO index has changed to a slight positive phase, which generates cooling of ocean waters (Wood et al. 2021). However, the cooling has not been strong enough to decrease the temperatures of the ocean water back to levels from the mid-1990's (Khazendar et al. 2019). Additionally, ocean waters are also warming due to anthropogenic climate change (Bindoff et al. 2013). Bindoff et al. (2019) found that the heat uptake in the upper ocean (0 - 700 m) was very likely higher for the period of 1993 - 2017 compared to 1969 - 1993.

We therefore explore whether or not some glaciers are more vulnerable to the warming of Baffin Bay Intermediate Water; the warmer waters of Atlantic origin. We first investigate the pathways of Atlantic Water along the shelf and through the canyon system. Then we study how the geometry of the fjordal channel network impacts the availability of waters of Atlantic origin at the glacier calving fronts. We also consider the fjord geometry and bed slope in the analysis. To our knowledge, these pathways of Atlantic originating waters from shelfbreak to the glacier calving fronts have not been considered in previous studies.

A new opportunity to understand the ocean-ice interactions around the Greenland Ice Sheet arose when NASA launched the Oceans Melting Greenland (OMG) mission to measure bathymetry, glacier elevation and physical properties of the ocean around the perimeter of the Greenland Ice Sheet in 2015 (Fenty et al. 2016). Additionally, Mankoff et al. (2020) published discharge estimates for the Greenland Ice Sheet glaciers with an ice flow faster than 100 m/yr. The newly obtained ocean topography data, combined with other data sources in BedMachine version 4 (BMv4) (Morlighem et al. 2017; Morlighem 2021), temporal availability of temperature and salinity profiles of the sea water and glacier ice discharge have given us the opportunity to study the importance of Atlantic Water pathways for understanding the discharge pattern in Northwest Greenland.

In addition, model data was made available from two sources; the HYCOM consortium and Alfred Wegener Institute (AWI). HYCOM is a HYbrid Coordinate Ocean Model that is globally available. Since the coordinate system is defined to be hybrid, it can change depending on the location. The coordinate is isopycnal in the open stratified ocean, it changes to a terrain following coordinate in more shallow coastal regions and reverts to z-level when in an unstratified sea (Chassignet et al. 2007). AWI developed the FESOM 1.4 model, a mature global sea-ice ocean model (Howat, Negrete, and Smith 2014) that utilizes an unstructured mesh containing triangular surfaces. It is mainly developed for large scale ocean circulation and climate research.

This thesis addresses the following questions:

1. What are the pathways of Atlantic Water in Northwest Greenland in space and time?
2. Are certain glaciers in Northwest Greenland more vulnerable to melting by deep water of Atlantic origin?
3. To what extent does the period of ocean warming correspond to the period of changing normalised discharge?
4. When the period of increased discharge does not correspond to the period of ocean warming, what then is the reason for the changing discharge?

In the following sections, we explain how the pathways of Atlantic Water are analysed in space in the canyons and the fjordal channel network using the FESOM model and CTD data (section 2.1) and in time using the HYCOM model (section 2.2); we present the derivation of the discharge change of glaciers (section 2.3.1), how the locations of glacier calving fronts are obtained (section 2.3.2) and the classification of bed slope and fjord geometry (section 2.3.3). In section 3.1 we describe the position of Atlantic Water in the canyons, the flow of Atlantic Water from FESOM (section 3.2) and from the CTD data (section 3.3). Furthermore we describe the temperature trends from HYCOM (section 3.4), determine which glaciers showed the biggest change in discharge over the warming period (section 3.5) and zoom in on these glaciers to determine their vulnerability to Atlantic Water pathways, by considering the depth of the bed, bed slope and fjord geometry (section 3.6). In chapter 4 we provide the discussion, followed by the conclusion in chapter 5 and finally, the recommendations in chapter 6.

2

Methods

To investigate the vulnerability of marine terminating glaciers to pathways of Atlantic Water, we first analysed the flow of Baffin Bay Intermediate Water in space using the FESOM model (Howat, Negrete, and Smith 2014) and CTD data from the OMG Mission (OMG Mission 2020b). In order to understand over which time period the Baffin Bay Intermediate Water warmed, we evaluated temperature at depth from the HYCOM model (Chassignet et al. 2007) in Baffin Bay and in the canyons that lead to the fjordal channel network. We tested the vulnerability of the glaciers to the Baffin Bay Intermediate Water by analysing the change in discharge over the warming period using discharge estimates from Mankoff et al. (2020) and considered the depth using bathymetry from BedMachine v4 (An et al. 2019) to assess whether there was a pathway for Baffin Bay Intermediate Water. The stability of the calving front was evaluated by determining the calving front positions in time and considering bed slope and fjord geometry.

The conducted analyses are summarised in Figure 2.1.

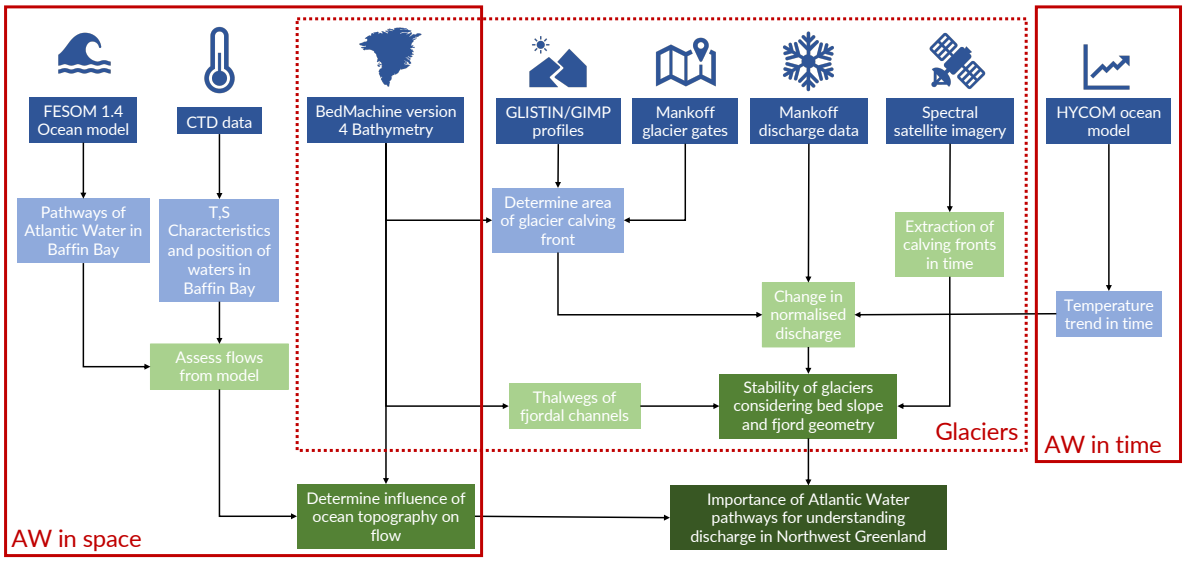

Figure 2.1: **Research Approach**. Research consists of three different parts. 1) The flow of Atlantic Water in space (outlined in in the box on the left), 2) the temperature trends of Atlantic Water in time (outlined in the box on the right) and 3) the vulnerability of glaciers to pathways of Atlantic Water.

2.1. Pathways of Atlantic Water in Baffin Bay

To investigate the pathways of Baffin Bay Intermediate Water along the shelf and through the canyon system, we used the FESOM model (Howat, Negrete, and Smith 2014). Daily model data from September 2019 was analysed. This period of one month was considered long enough to capture the spatial off-the-shelf/on-the-shelf pathways of Atlantic Water at depth. In addition, September 2019 was chosen in order to compare it to the Conductivity, Temperature, Depth (CTD) profiles of the ocean, which were obtained during the OMG Mission in September 2019.

The model resolution of roughly 9 km, allowed for reliable solutions up to the fjordal channel network. The direction of the flow along the shelfbreak and the effect of topographic steering in the canyons was assessed by creating videos of potential temperature and salinity for each depth level up to 580 m (0-100 m with a 10 m interval, 115, 135, 160, 190, 230, 280, 340, 410, 490, 580 m).

To evaluate the flows at depth of the FESOM model in the canyons, CTD data from the OMG Mission was used (OMG Mission 2020a). The Baffin Bay Intermediate Water was isolated in each CTD profile through classification of the water body. The definition of Baffin Bay Intermediate Water from Gladish, Holland, and Lee (2015) was utilised (Equation 2.1).

$$\begin{aligned} &27.4 \leq \sigma_\theta \leq 27.675 \\ &\theta \geq \frac{3.0-0.5}{27.675-27.4}(\sigma_\theta - 27.4) + 0.5 \\ &\theta \leq 3.0 \end{aligned} \tag{2.1}$$

Baffin Bay Intermediate Water was defined by Gladish, Holland, and Lee (2015) in potential temperature (θ) and potential density anomaly (σ_θ) space. However, the CTD data consisted of in-situ temperature and conductivity measurements. These measurements were converted to potential temperature and potential density anomaly using the Thermodynamic Equation of Seawater (TEOS-10) (Feistel 2008), for each separate profile. A detailed description of this conversion can be found in Appendix B.

The CTD data was available over the period 2016 - 2020, with a temporal resolution of one year. Six profiles were obtained in the Southern canyon and eleven profiles in the Northern canyon during the OMG Mission. Even though the temporal and spatial resolution were sparse, CTD data could still be used to obtain a detailed picture of the depth at which the Baffin Bay Intermediate Water was present and give an indication of existing currents and circulation.

Currents were detected by investigating the spatial temperature differences of classified Baffin Bay Intermediate Water between the profiles in time. For each profile, the mean temperature of Baffin Bay Intermediate Water was calculated. Then the temperature differences between the profiles for each timestep were analysed. A current indicated by FESOM was thought to exist if a specific profile was persistently warmer or colder compared to the other CTD profiles in time and coincided with the location of a detected current in FESOM.

In addition, CTD data was used to evaluate the bias and offset of the FESOM model. Cross sections of potential temperature (θ) and practical salinity (SP) were acquired from the FESOM model and the CTD data. To properly compare the model with the data, model sections were taken from the acquisition date of the CTD's and in corresponding locations. A detailed description of the comparison can be found in Appendix C. We observed that the FESOM model had a bias of +2.5°C in temperature and an offset of about +100 m considering the depth of Baffin Bay Intermediate Water.

Since the FESOM model was only used to determine the pathways of Atlantic Water in space and the flow that is displayed by the model was realistic, the bias and offset do not pose a problem.

We choose to use the FESOM model for spatial analysis instead of the HYCOM model for one main reason. The HYCOM model showed currents in the Northern and Southern canyon that did not correspond to the theory of topographic steering. Figure 2.2 shows a mean outflow from both the Southern and Northern canyon, while considering theory an inflow is expected. From the shelf-break to the canyon, the depth of the bed decreases. As a result the Coriolis force has to decrease and the flow is deflected towards the equator and thus into the canyons, which is the opposite to what is displayed by HYCOM.

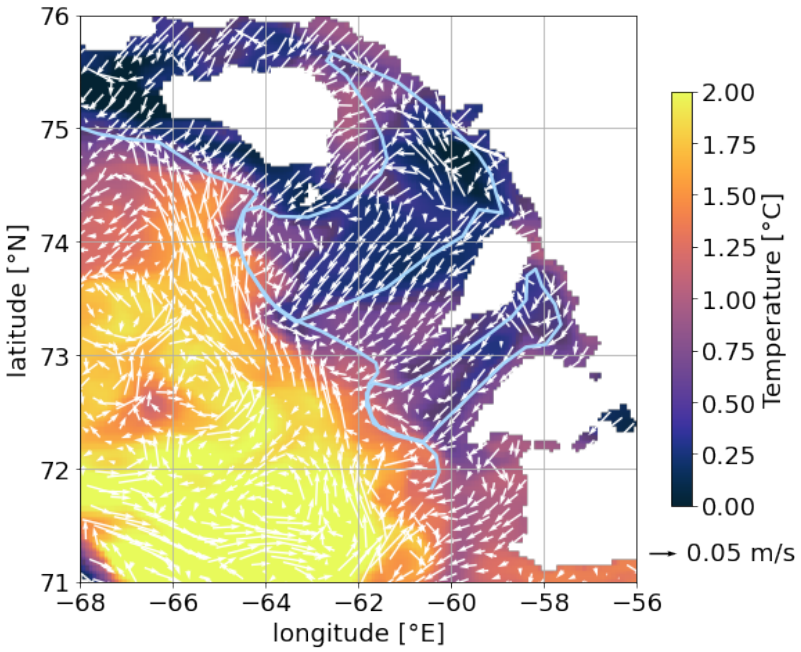

Figure 2.2: **Mean HYCOM model temperature and currents at 300 m depth**. Mean HYCOM temperature, currents from September 2019. Northern canyon, Southern canyon and shelfbreak are outlined in light blue.

2.2. Decadal temperature trends of Atlantic Water in Baffin Bay

To understand over which time period the Baffin Bay Intermediate Water warmed, we evaluated temperature at depth from the HYCOM model for ten locations in Davis Strait, Baffin Bay and in the canyons that lead to the fjordal channel network. Tang et al. (2004) found water of Atlantic origin between 300 - 800 m. Therefore we considered the depth levels 300 m, 350 m, 400 m, 500 m, 600 m, 700 m and 800 m from the HYCOM model.

Water of Atlantic origin reaches Baffin Bay through the Davis Strait and is known to move along the shelfbreak into the canyons. Therefore we selected two points at the beginning and the end of the Davis Strait, four points along the shelfbreak and two points in each canyon. Around each point a buffer of 1000 m was added to filter out as many uncertainties from HYCOM as possible.

Since the NAO negative phase, which is associated with ocean warming, was persistent from the mid-1990's to 2010 (Wood et al. 2021), the HYCOM model temperatures were considered between 1993 - 2018. We obtained monthly mean temperatures from 50 m scaled HYCOM data for each buffered point at each depth level.

2.3. Glaciers

To test the vulnerability of the glaciers to the Baffin Bay Intermediate Water, we analysed the change in normalised discharge over the warming period using discharge estimates from Mankoff et al. (2020). The glaciers that showed the highest normalised discharge change were analysed further. The normalised discharge estimates in time were analysed and since warming of Baffin Bay Intermediate Water is known to initiate retreat, the calving front positions of the highest discharging glaciers were obtained between 1989 - 2021. In addition, the availability of the Baffin Bay Intermediate Water at the glaciers front depends on the depth of the bed. Therefore bathymetry from BedMachine v4 was obtained in the fjordal channels (Morlighem et al. 2017; Morlighem 2021). Furthermore, the stability of the calving front depends on the thickness of the glacier, the bed slope and fjord geometry (Bunce et al. 2018), which we assessed qualitatively.

In section 2.3.1 the derivation of the discharge change is outlined, 2.3.2 summarises the process of obtaining calving fronts and section 2.3.3 describes the classification of the bed slope and fjord geometry as well as the extraction of the fjordal channel depth.

2.3.1. Discharge change

The effect of warming on the discharge estimates was determined by calculating the change in normalised discharge over the warming period for each glacier in Northwest Greenland with a depth (below sea level) of at least 100 m. We assume that glaciers more shallow than 100 m are not impacted by warm Atlantic water. A five year block before the initiation of warming was selected and a five year block after the end of warming. For each block the mean normalised discharge was calculated. Then the five year normalised discharge mean before warming ($\overline{Q}_{\text{norm, 5 years, before}}$) was subtracted from the five year normalised discharge mean after warming ($\overline{Q}_{\text{norm, 5 years, after}}$) to get the change in normalised discharge (ΔQ_{norm}), see Equation 2.2.

$$\Delta Q_{\text{norm}} = \overline{Q}_{\text{norm, 5 years, before}} - \overline{Q}_{\text{norm, 5 years, after}} \tag{2.2}$$

We normalised the discharge estimates of each glacier by the glacier's calving front area, such that we obtained discharge per unit area (Gt/km^2). We took this approach to prevent the estimates from being biased towards glaciers with large fronts. That is, deep wide glacier fronts would naturally show higher discharge estimates compared to deep narrow fronts if ice flow velocity was similar. Therefore, using normalised discharge change allowed for easy detection of extreme changing glaciers regardless of their size.

We calculated normalised discharge (Q_{norm}) using Equation 2.3. Where Q_{gate} is the discharge estimate of each gate and A_{gate} is the gate cross sectional area. We obtained discharge estimates (Q_{gate}) from Mankoff et al. (2020). They defined discharge through glacier gates, which are positioned 5 kilometers upstream for the baseline termini.

$$Q_{\text{norm}} = \frac{Q_{\text{gate}}}{A_{\text{gate}}} \tag{2.3}$$

To determine the gate cross sectional area (A_{gate}), we used Equation 2.4. Here l_{pixel} is the length of each pixel and ($\overline{h}_{\text{GLISTIN/GIMP},i} - \overline{d}_{\text{BMv4},i}$) represents the thickness of the glacier per pixel. We obtained glacier grounding depth ($\overline{d}_{\text{BMv4}}$) from Bedmachine version 4 (Morlighem et al. 2017; Morlighem 2021). Glacier elevation ($\overline{h}_{\text{GLISTIN/GIMP}}$) was derived from GLISTIN (high resolution Airborne Glacier and Ice Surface Topography Interferometer) in 2019 (OMG Mission 2020a). If GLISTIN elevations were not available, GIMP (Greenland Mapping Project) was used, which had a nominal date of 2007

(Howat, Negrete, and Smith 2014). We used gate locations from Mankoff et al. (2020), the gates are defined in pixels with a standard width of 200 m, while length (l_{pixel}) varied per pixel (see Figure 2.3). Thus, the pixels do not have a regular size, the area of each pixel can differ. We determine $\overline{d}_{\text{BMv4}}$ and $\overline{h}_{\text{GLISTIN/GIMP}}$ for each gate pixel i.

$$A_{\text{gate}} = \sum_{i=1}^{n} l_{\text{pixel},i} \cdot (\overline{h}_{\text{GLISTIN/GIMP},i} - \overline{d}_{\text{BMv4},i}) \tag{2.4}$$

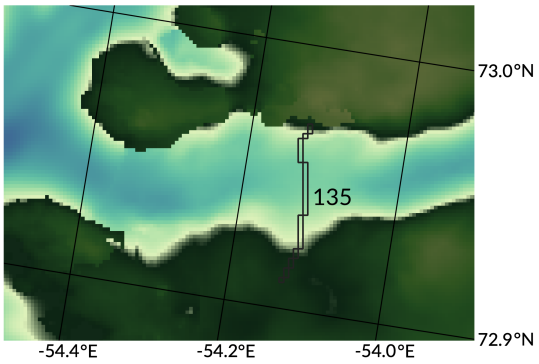

Figure 2.3: **Pixels of glacier gate 135.** Glacier gate 135 (Upernavik C) pixels outlined in black have a standard width of 200 m and varying length. Thus the pixels do not have a regular size. Pixels are shown on top of BMv4 data. Each black outlined gate pixel can contain a different amount of BMv4 pixels.

The error of normalised discharge change ($e_{\Delta Q_{\text{norm}}}$) was fourfold and consisted of BMv4, GLISTIN, GIMP and discharge. Since Mankoff et al. (2020) took the error of BMv3 and GIMP into account in its discharge error and BMv4 is an improved version of BMv3, we did not add them again. The additional error from GLISTIN was obtained per gate pixel (Equation 2.5). Then the error of the cross sectional area per gate was calculated by weighing the error on the GLISTIN pixel count (Equation 2.6). This was needed because of the varying pixel size. The discharge error for each five year block was determined by taking the square sum over the error of each timestep divided by the number of timesteps (Equation 2.7). Next, the discharge change error was obtained by taking the square sum of the discharge error of both five year blocks (Equation 2.8). Finally, the discharge change- and area error were combined to get the discharge change error per gate (Equation 2.9).

$$e_{\text{A,pixel}} = \sqrt{\frac{\sum_{i=1}^{n} e_{\text{GLISTIN},i}^2}{\sum w_i}} \tag{2.5}$$

$$e_{\text{A}} = \sqrt{\frac{\sum_{i=1}^{n} w_i \cdot e_{\text{A,pixel},i}}{\sum_{i=1}^{n} w_i}} \tag{2.6}$$

$$e_{\overline{Q}} = \sqrt{\frac{\sum_{t=1}^{n} e_{Q,t}^2}{\sum_{i=1}^{n} t}} \tag{2.7}$$

$$e_{\Delta Q} = \sqrt{e_{\overline{Q},\text{5 years, before}}^2 + e_{\overline{Q},\text{5 years, after}}^2} \tag{2.8}$$

$$e_{\Delta Q_{\text{norm}}} = \Delta \overline{Q}_{\text{norm}} \cdot \sqrt{\left(\frac{e_{\Delta \overline{Q}}}{\Delta Q_{\text{norm}}}\right)^2 + \left(\frac{e_A}{A}\right)^2} \tag{2.9}$$

We observed that elevations from GIMP and GLISTIN per glacier could be significantly different. This difference propagated into the estimate of the calving front area and therefore also into the

estimate of discharge change. Thus, the absolute difference between the GIMP- and GLISTIN discharge change estimates was added as an addition error source (see Equation 2.10).

$$e_{\Delta Q_{\text{norm, all}}} = e_{\Delta Q_{\text{norm}}} + |\Delta Q_{\text{norm, GLISTIN}} - \Delta Q_{\text{norm, GIMP}}| \tag{2.10}$$

2.3.2. Retreat

To investigate the effect of retreat on the discharge estimates of the glaciers that showed the highest normalised discharge change, we created false colour composites to derive the calving front positions between 1989 - 2021. We used optical imagery from Landsat- 5, 7 and 8 and Sentinel 2 satellites.

We filtered the optical imagery on time and on cloud cover. The summer months, June to September, were selected for each year because of the longer daylight and thus a higher amount of useful images. In addition, we wanted to derive the calving fronts from the same season to fairly compare the results. We filtered the images on 20% cloud cover or less to maximize the chance of a cloud free calving front. This simplified the calving front extraction process.

Table 2.1: **Overview of bands used in the false colour composites per satellite**.

		Band number per satellite			
Visualization	**Band description**	**Landsat 5**	**Landsat 7**	**Landsat 8**	**Sentinel 2**
Red	Red	B3	B3	B4	B4
Green	NIR	B4	B4	B5	B8
Blue	SWIR	B5	B5	B6	B11

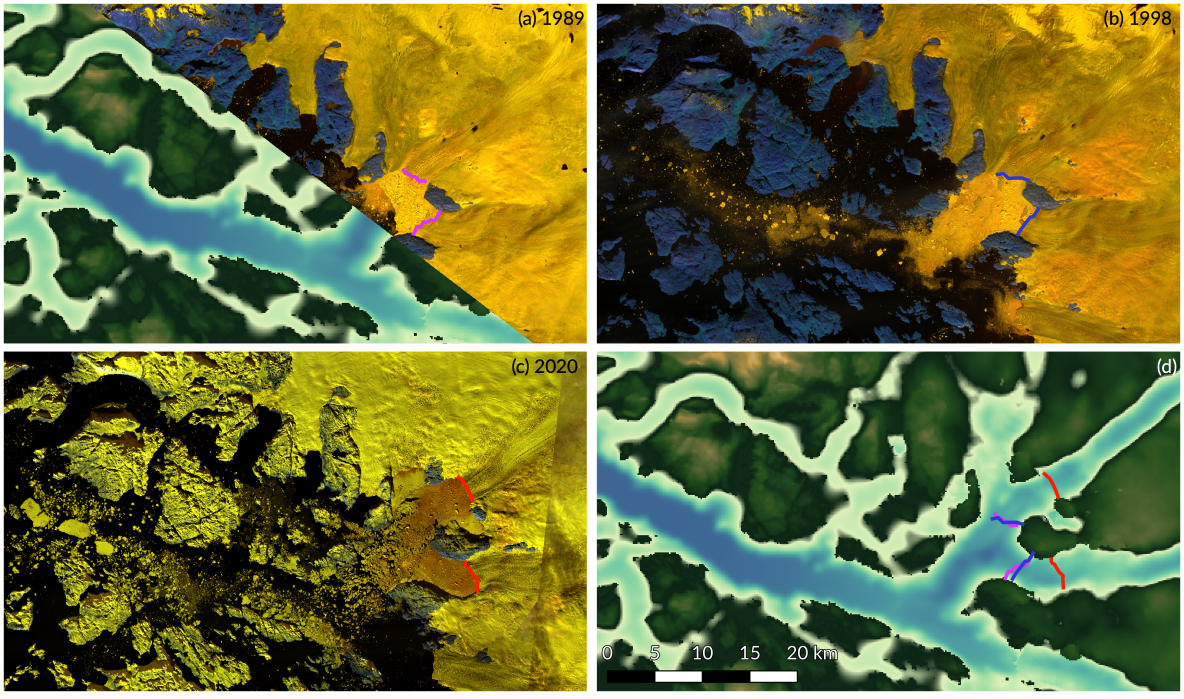

Figure 2.4: **Optical imagery of Upernavik calving fronts in time**. **(a)** Landsat 5 false color composite from 1989, calving fronts are outlined in pink. **(b)** Landsat 5 false color composite from 1998, calving fronts outlined in blue **(c)** Sentinel 2 false color composite from 2020, calving fronts are outlined in red. **(d)** Bathymetry of Upernavik fjordal channels with calving front outlines from 1989, 1998 and 2020 on top.

To further facilitate the easy extraction of calving fronts, we created false colour composites. With this approach the difference between the ice of the calving front and the ocean water was maximized. Multispectral instruments, such as Landsat- 5, 7 and 8 and Sentinel 2, pick up the intensity of reflected wavelengths from Earth in bands with specific ranges. They include the visible Red, Green and Blue bands but also Near InfraRed (NIR), ShortWave InfraRed (SWIR) and Thermal InfraRed (TIR) bands. Here a combination of the Red, NIR and SWIR band was used. The Red band was visualised in red, the NIR band in green and the SWIR band in blue, an overview per satellite can be found in Table 2.1. Figure 2.4 shows three of the created false colour composites highlighting how calving fronts were extracted from the images.

2.3.3. Fjordal channel depth, fjord geometry and bed slope

To test if Baffin Bay Intermediate Water had a direct pathway to the calving fronts, we calculated the depth of each glacier gate and extracted thalwegs (lines that represent the deepest part of a channel) from the fjordal channels towards the glacier calving fronts that showed the highest normalised discharge change. We calculated mean depth using Equation 2.11. Since l_{pixel} varies from gate pixel to gate pixel as visualised in Figure 2.3, we weighted the mean depth by the amount of BMv4 pixels within a gate pixel.

$$\overline{d}_{BMv4} = \frac{\sum_{i=1}^{n} w_i \cdot d_{BMv4,i}}{\sum_{i=1}^{n} w_i} \tag{2.11}$$

To determine the vulnerability of the glaciers to Baffin Bay Intermediate Water, we also took into consideration the stability of the calving front. How fast a glacier retreats depends on the thickness of the glacier, the bed slope and fjord geometry (Bunce et al. 2018). We assessed them qualitatively using the classification of fjord geometry from Carr, Stokes, and Vieli (2014) (Figure 2.5) and bed slope from Bunce et al. (2018) (Figure 2.6) over the full retreat distance of the glacier.

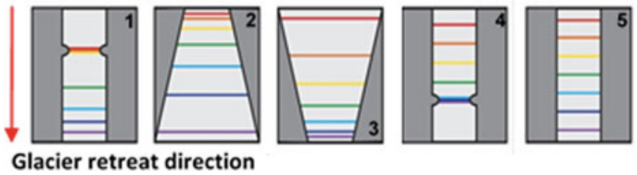

Figure 2.5: **Classification categories used for fjord geometry. Figure 2 from Bunce et al. (2018), who adjusted it from Carr, Stokes, and Vieli (2014).** **(1)** Retreat from a lateral pinning point. **(2)** Retreat into a widening fjord. **(3)** Retreat into a narrowing fjord. **(4)**. Retreat onto a lateral pinning point. **(5)** Parallel retreat.

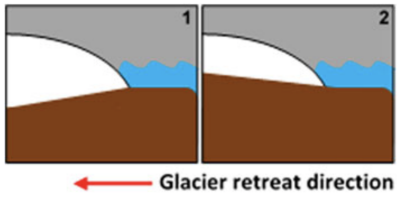

Figure 2.6: **Classification categories used for bed slope. Figure 3 from Bunce et al. (2018).** **(1)** reverse bed slope. **(2)** normal bed slope.

3

Results

3.1. Position of Atlantic Water in canyons

Water originating from the Atlantic Ocean, referred to as Baffin Bay Intermediate Water (BBIntW), is found in every CTD profile in the Southern and the Northern canyon (Figure 3.1a) and is therefore assumed to be present throughout both canyons. From the CTD profiles in the Southern canyon we derive that BBIntW is found between 252 and 426 m on average. In the Northern canyon we find BBIntW between 261 and 419 m. In addition, we identify that BBIntW is indeed the warmest water body at depth in both canyons (Figure 3.1b).

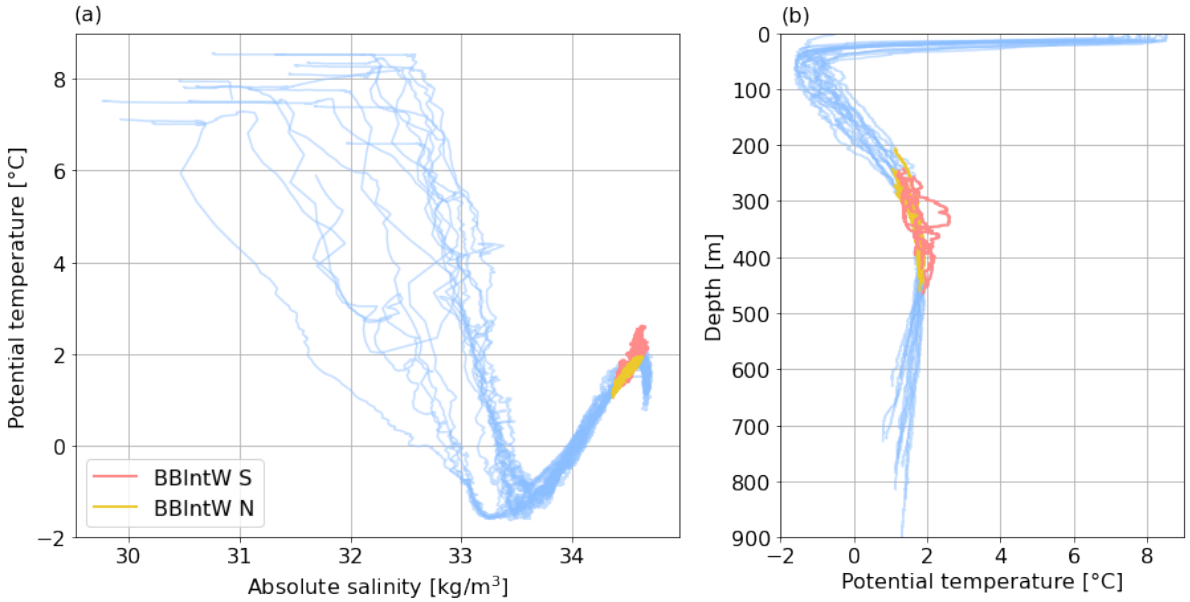

Figure 3.1: **Potential temperature and absolute salinity of CTD profiles from both the Southern and Northern canyon.** **(a)** Potential temperature and salinity plot from 2019 AXCTD data. The location of BBIntW in the Southern canyon (BBIntW S - light red) and in Northern canyon (BBIntW N - golden yellow) is highlighted. **(b)** Potential temperature over depth indicating the depth of BBIntW in the Southern and Northern canyon.

3.2. Flow of Atlantic Water from FESOM

From Figure 3.2a we detect that Baffin Bay Intermediate Water, which enters Baffin Bay through the Davis Strait, moves northward with a shelfbreak current. The position of the shelfbreak current in the FESOM model corresponds to the location of the anti-cyclonic boundary current that flows around Baffin Bay as described by Fenty et al. (2016).

We identify a second current that flows along the second break in the topography, the transition from the canyon head to the fjordal channel network, which we define as the inner shelfbreak. Just like the shelfbreak current, the inner shelfbreak current moves northward. It bends towards the East to follow the Northwest Greenland coastline at the Northern end of the Northern canyon head.

Both the shelfbreak and inner shelfbreak current are bounded by the topography, but when the shelfbreak current reaches the mouth of the Southern canyon, the depth of the ocean floor decreases (Figure 1.3). As a result, the Coriolis force has to decrease and therefore a part of the shelfbreak flow is steered into the mouth of the Southern canyon. At the mouth of the Northern canyon we detect the same steering effect. In both canyons the flow continues its path towards the head of each canyon (solid lines in canyons in Figure 3.2b).

At the head of both canyons, we identify that the flow continues in three directions. Circulation in the canyon results in a return current that moves back to the mouth of the canyon, where it will flow out into the shelfbreak current (dashed line). It can join the inner shelfbreak current (solid line) or it can continue its path straight into a fjordal channel (dotted line).

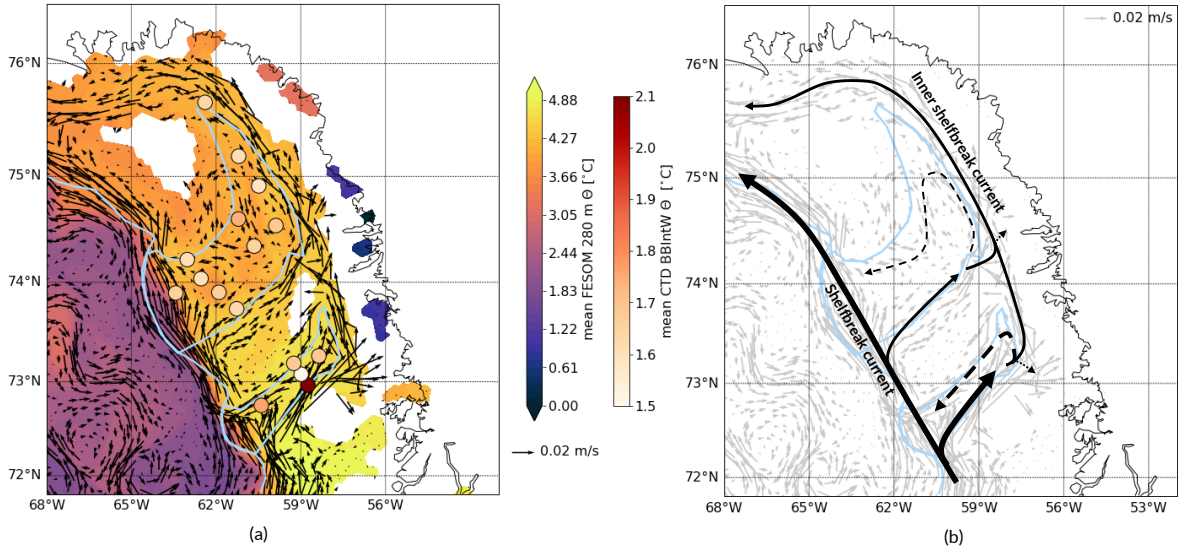

Figure 3.2: **Potential temperature and currents at 280 m depth from FESOM, CTD BBIntW mean potential temperature**. **(a)** Mean FESOM temperature and currents from September 2019. Northern and Southern canyon are outlined in light blue. In the Southern and Northern canyon we show mean BBIntW potential temperature from CTD data 2019 (Fenty et al. 2016). **(b)** Diagram showing the main flows in the Southern and Northern canyon. Solid lines indicate inflow into canyons, dashed lines the return flow and dotted lines the pathway to the Upernavik and Alison fjordal channel. Thickness of lines indicates the strength of the flow. Grey arrows in the background are mean currents from FESOM from September 2019.

When comparing the Southern and Northern canyon, we notice that both the strength of the inflow at the mouth and outflow of the return current are different. Both the inflow (solid line) and outflow (dashed line) in the Southern canyon are faster, indicating that the currents are stronger. In addition, we recognise that the width of the canyons differs. When measured at the center of each canyon, we find that the Northern canyon has a width of approximately 90 km and the Southern canyon of about 30 km. We hypothesize that this width difference influences the flow strength.

In Figure 3.2a we also detect a difference in the Baffin Bay Intermediate Water temperatures obtained from the CTD profiles in both canyons. In the Southern canyon, one CTD profile has significantly warmer Baffin Bay Intermediate Water (dark red) compared to the other CTD locations (white to light orange). Such a contrast is absent in the BBIntW CTD temperatures in the Northern canyon.

3.3. Flow of Atlantic Water from CTD data

The warmest Baffin Bay Intermediate Water in the Southern canyon is detected in CTD profile 472 in 2019 (Figure 3.3a). The other five CTD profiles in the Southern canyon show colder Baffin Bay Intermediate Water relative to profile 472. The contrast in temperature in the canyon is also apparent in the cross canyon section displayed in Figure 3.3b. Here a warm patch (outlined in green) is clearly detected at depth at the location of profile 472. A warm patch is missing at the position of CTD profile 468.

In Figure 3.3c we identify that the temperature of Baffin Bay Intermediate Water observed in profile 472 (outlined in green) is warmer than all the other profiles in each timestep between 2016 and 2020. In addition, we find that the warm patch at depth at the location of profile 472 is present in each cross canyon section between 2016 and 2020 (see Appendix C). Thus, The Baffin Bay Intermediate Water at the South side of the Southern canyon is persistently warmer compared to its surroundings in time.

The position of CTD profile 472 corresponds to the location where a strong warm topographically steered inflow is detected in the FESOM model results (section 3.2). The fact that this CTD profile is persistently warmer than its surroundings over a five year period proves that indeed such an inflow of warm water at depth is present.

At the head of the Southern canyon, the warm strong inflow may continue its path into a fjordal channel. At the South side of the canyon head, the Upernavik fjordal channel has its entrance. In Figure 3.3a we detect that CTD profile 470, which is located in the Upernavik fjordal channel, is warmer than all CTD profiles in the Southern canyon except for profile 472. Therefore, we find that the Baffin Bay Intermediate Water in profile 470 can only originate from profile 472. The Baffin Bay Intermediate Water observed in the other CTD profiles is too cold to be the source. This proves that the strong topographically steered inflow of Baffin Bay Intermediate Water in the Southern canyon thus continues its path into the Upernavik fjordal channel.

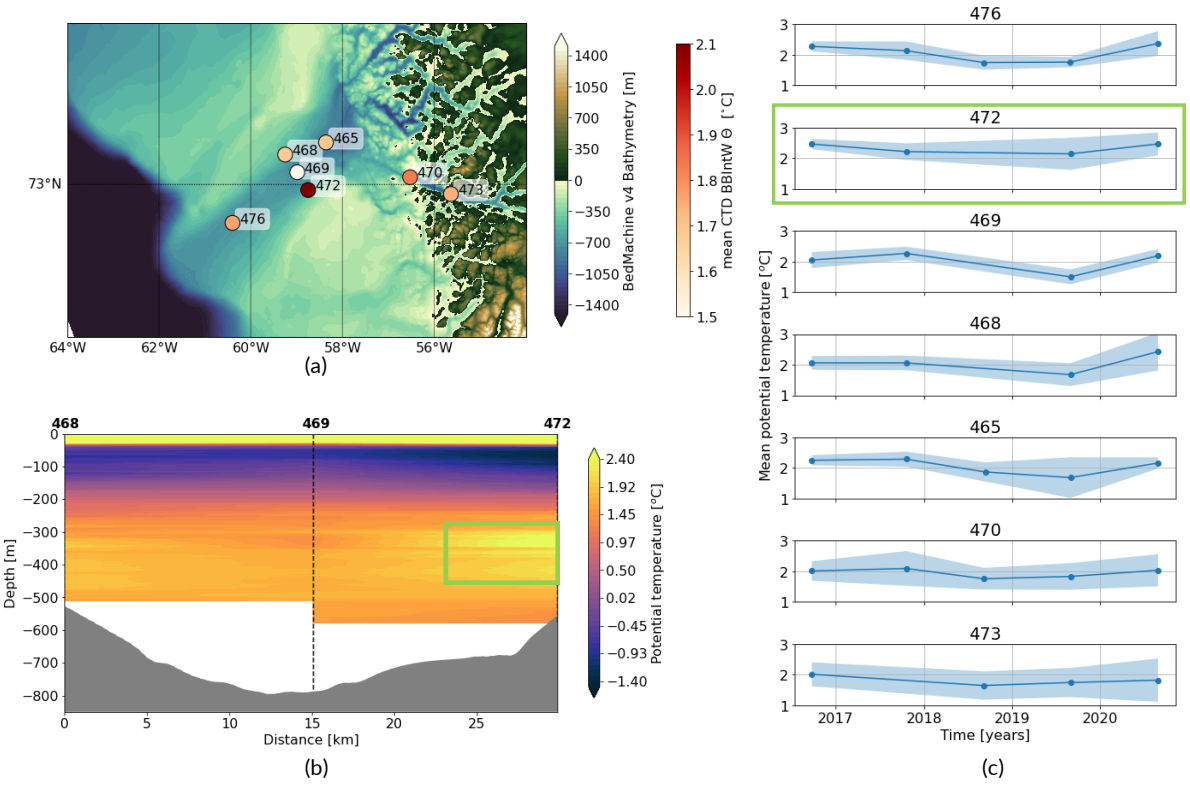

Figure 3.3: **CTD (BBIntW) temperature of Southern canyon and Upernavik channel. (a)** BBIntW mean potential temperature from CTD data obtained in 2019. Background map is bathymetry (Morlighem et al. 2017; Morlighem 2021). **(b)** Cross section of potential temperature obtained from CTD probes 468, 469, 472 in 2019 across the Southern canyon, the warm patch is indicated by the green box. At the white area interpolation between CTD profiles was not possible due to depth differences. **(c)** CTD BBIntW mean potential temperature over the period 2016-2020, shaded area is the 95% confidence interval. Upper five plots are from the Southern canyon, lower two plots are from fjordal channel leading to the Upernavik glacier gates (134, 135, 136). Numbers correspond to numbers in (b).

3.4. HYCOM temperature trends at depth

The deep waters of Atlantic origin cool when they move northward. Moving from location 1 to location 6, we observe that the temperature of water at depth decreases and that the temperature fluctuations dampen (Figure 3.4). Fenty et al. (2016) relate the observed cooling to the process of lateral mixing and exchange with the relatively colder waters that are positioned on top of warm Atlantic Water during its transit northward.

We analyse that the temperature of the deep water of Atlantic origin in Baffin Bay and the canyons (location 2 - 10) can be split up into three periods based on the temporal trends. A stable period with a relatively constant temperature between 1993 - 1996. A period of rapid warming in 1997 - 2011 and a relatively slow cooling period between 2012 - 2018 (Figure 3.4b, c). In the Davis Strait (location 1), the three periods can be distinguished, but the differences between the three periods are not as clear compared to location 2 - 10.

Within the warming period (1997 - 2011) we identify three cycles of relative warming and cooling. The first and longest cycle is between 1997 - 2002, we detect the second cycle from 2003 to 2006 and the final cycle is found between 2007 - 2011.

When we compare the temperature trends of the Southern and the Northern canyon, we find that the temperatures observed in the Southern canyon over all depths are slightly higher. The difference in temperature increases when moving to deeper depths. We also find a delay in the temperature trend. The warming in the Southern canyon started 6 to 8 months earlier compared to the Northern canyon according to the HYCOM model.

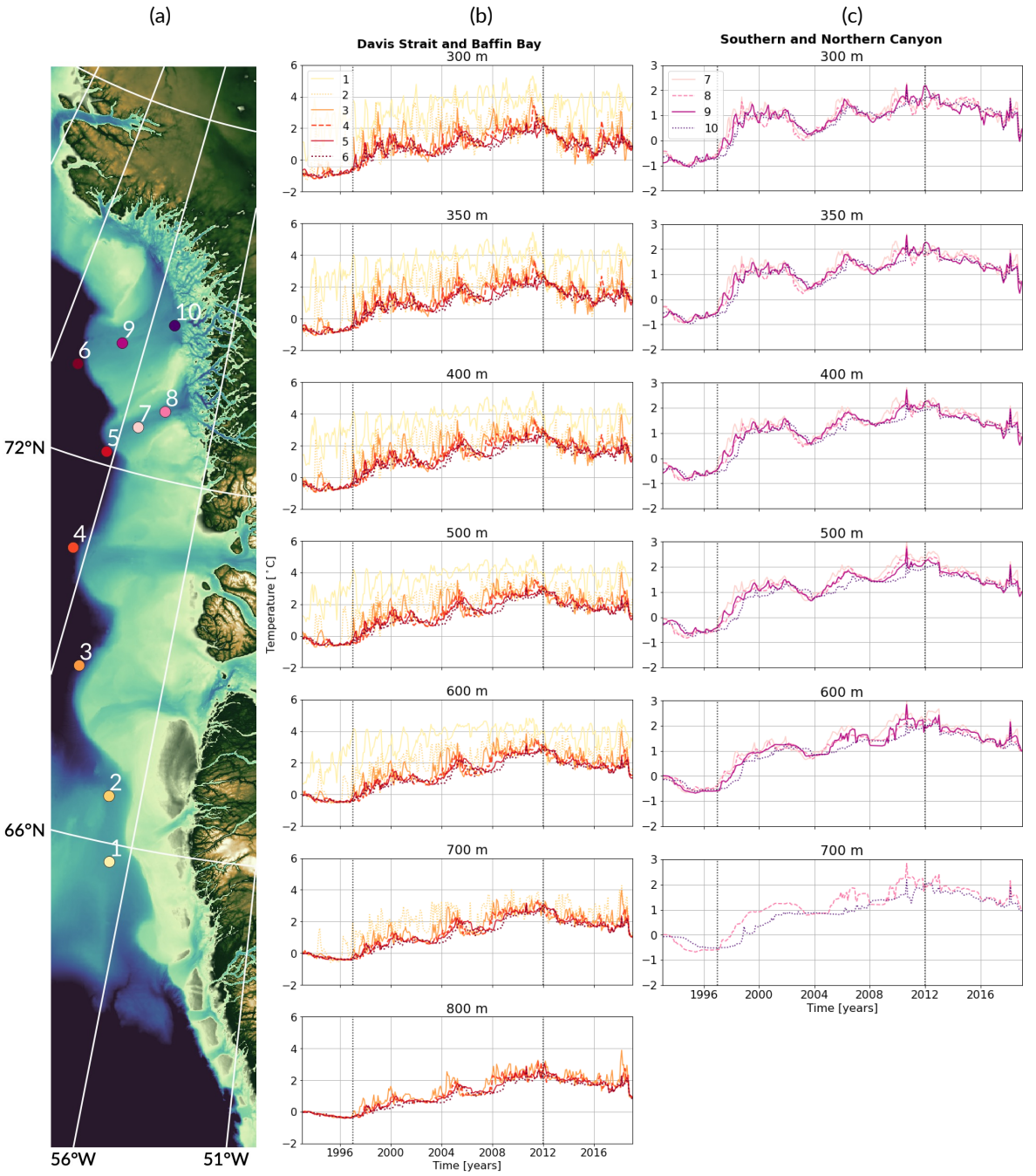

Figure 3.4: **HYCOM temperature trends at depth**. **(a)** Overview of locations where HYCOM temperatures were obtained. **(b)** Temperature trends from 1993 - 2018 for 300, 350, 400, 500, 600, 700, 800 m depth levels in Davis Strait (location 1 and 2) and Baffin Bay (location 3 to 6). Each colored trend corresponds to a location number displayed in the legend and on the map in (a). The colors of the trends corresponds to the colors displayed in the map. **(c)** Temperature trends in Southern (location 7 and 8) and Northern canyon (location 9 and 10). Vertical dotted lines indicate the observed warming period.

3.5. Glacier discharge change

Normalised discharge change over the warming period ($\Delta Q_{\text{norm}} = \overline{Q}_{\text{norm, 2012-2017}} - \overline{Q}_{\text{norm, 1991-1996}}$) in Northwest Greenland ranges between a decrease of -0.32 ± 0.01 Gt/km^2 and an increase of 1.31 ± 0.33 Gt/km^2 (Figure 3.5). We find that the magnitude of positive ΔQ_{norm} is larger than that of negative ΔQ_{norm}. The net change in discharge is larger for glaciers that show increasing discharge compared to glaciers that show decreasing discharge. As a result, the total normalised discharge of glaciers with a gate depth of at least 100 m in Northwest Greenland increased from 83.5 ± 1.1 Gt/km^2 to 101.2 ± 0.9 Gt/km^2 between the periods 1991-1996 and 2012-2017. In addition, we identify that 28 of the 40 analysed glaciers show an increase in normalised discharge over the warming period ($\Delta Q_{\text{norm}} > 0$). Thus, the majority (70%) of the glaciers is discharging more after the warming period ended.

In addition, we determine that there is no clear correlation between ΔQ_{norm} and the depth of the glacier gates. The deepest glaciers do not show the biggest change in normalised discharge. Notably, we even detect that some deep glacier gates (100 and 102) show a decrease in normalised discharge over the warming period. Since the Baffin Bay Intermediate Water is found at depth, we expected that deeper glacier were more exposed to the BBIntW and therefore more vulnerable. This result indicates that the depth of the glacier gate alone does not tell the complete story.

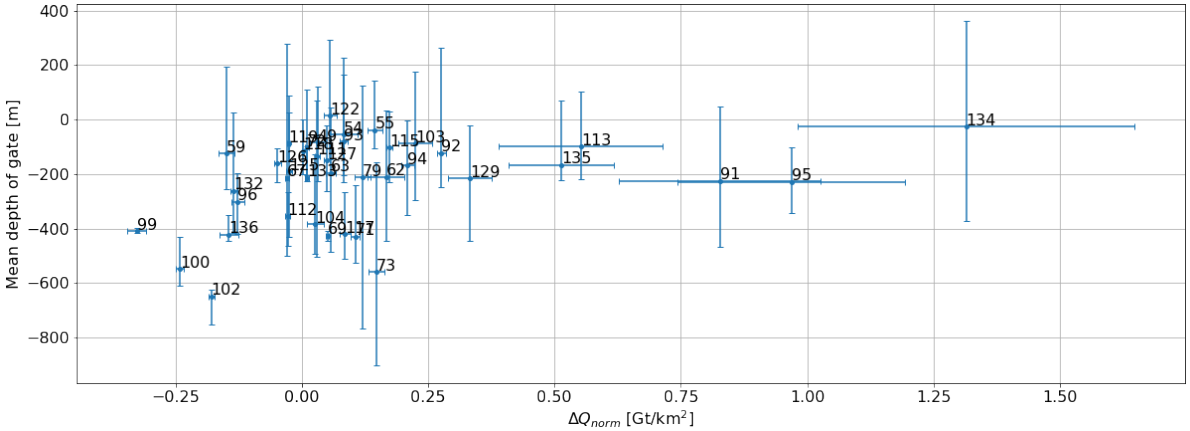

Figure 3.5: **Depth of glacier gates and change in normalised discharge over the warming period**. Overview of depth versus normalised discharge change of the 40 glaciers. The normalised discharge change is taken as the mean normalised discharge over the period 2012 - 2017 subtracted by the mean normalised discharge over the period 1991 - 1996 ($\overline{Q}_{norm,2012-2017}$ - $\overline{Q}_{norm,1991-1996}$). The bars on the vertical axis indicate the minimum and maximum glacier gate depth, the bars on the horizontal axis indicate the error in the normalised discharge.

Five glaciers exceed 0.5 Gt/km^2 normalised discharge change over the warming period (Figure 3.5). We observe the biggest change at Upernavik N (134), Kjer (95), Sverdrup (91), Alison (113) and Upernavik C (135) glacier gates. Upernavik N and Upernavik C are connected to the same fjordal channel and receive water from the Southern canyon. Kjer, Sverdrup and Alison all have seperate fjordal channels and receive water from the Northern canyon.

The ΔQ_{norm} pattern varies significantly from glacier to glacier (Figure 3.6), similar to the pattern of retreat (Murray et al. 2015). However we find two clear spatial clusters of positive ΔQ_{norm}. The first cluster includes gate 129 - 135, which have their fjordal channel entrances connected to the Southern canyon. The second cluster comprises gate 91 - 115, which have their fjordal channels attached to the Northern canyon. Northward from gate 91, ΔQ_{norm} is smaller in magnitude.

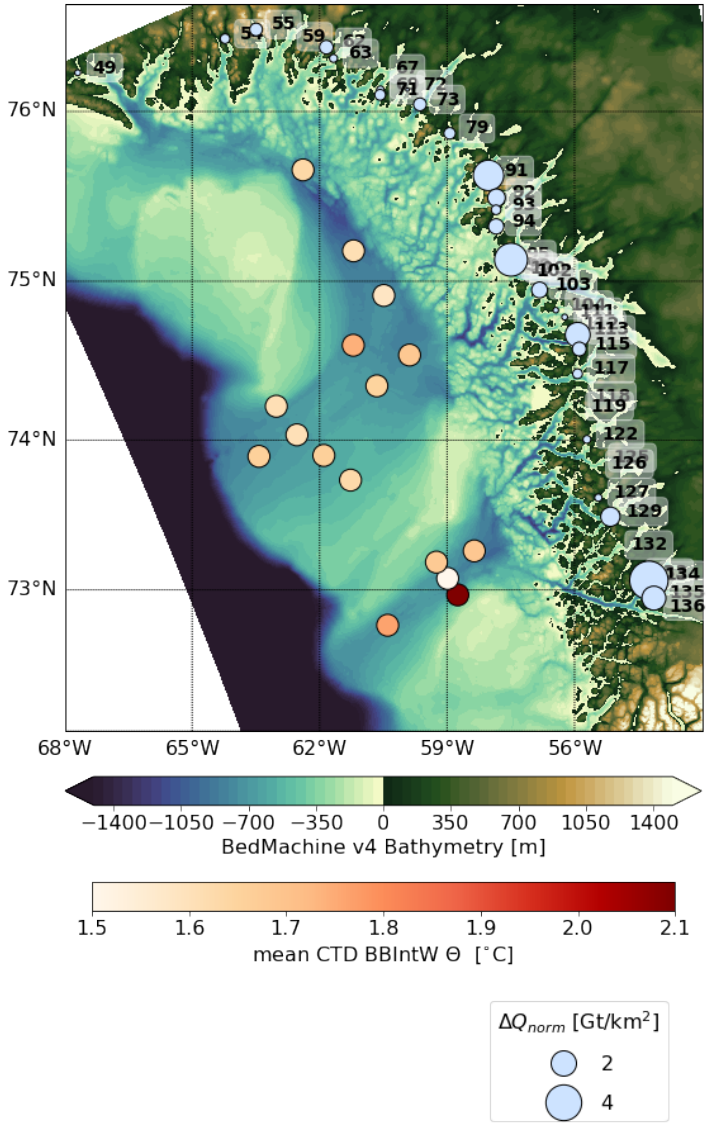

Figure 3.6: **Spatial distribution of glaciers normalised discharge change and CTD BBIntW mean potential temperature.** Northwest Greenland glaciers with an ice flow faster than 100 m yr^{-1} (Mankoff et al. 2020), have a depth of at least 100 m and show an increase in discharge over the warming period (28 glaciers). Circles proportional to the change in normalised discharge. Background is bathymetry (Morlighem et al. 2017; Morlighem 2021). In the Southern and Northern canyon we show mean BBIntW temperature from CTD data 2019.

3.6. Impact of fjord geometry and bed slope on glacier discharge

The five glaciers (Upernavik N, Kjer, Sverdrup, Alison and Upernavik C) that exceed 0.5 Gt/km^2 normalised discharge change are summarised in Table 3.1. Upernavik N (136) showed the largest retreat over the warming period, followed by Kjer (95), Sverdrup (91), Alison (113) and Upernavik C (135).

Upernavik N (136) experienced the biggest change in discharge over the warming period compared to all the other glaciers. In addition, we find that the fjordal channel is deep enough (> 500 m) to be a pathway for BBIntW (Figure 3.7a.2). The BBIntW can thus impact the glacier calving front. We also detect that the period of changing discharge corresponds to the period of ocean warming (Figure 3.8a.3).

The glacier started its retreat on a normal bed into a widening fjord (Figure 3.7a.1, Figure 3.8a.3). During its retreat the bed alternated between a normal and reverse slope. In 2009, 2 years before the end of the warming period, the fjord geometry of Upernavik N changed and the glacier started retreating onto a lateral pinning point and later showed parallel retreat. We hypothesize that the fast increase in discharge stopped once the geometry of the fjord changed.

Table 3.1: **Normalised discharge change, retreat and depth for five glaciers that exceed 0.5 Gt/km^2 in discharge change**. Normalised discharge change (ΔQ_{norm} = $\overline{Q}_{norm,2012-2017}$ - $\overline{Q}_{norm,1991-1996}$ [Gt/km^2]) is displayed including its error. Retreat from before warming (< 1997) to 2020/2021. Mean depth is displayed with its weighted standard deviation.

Gate	Glacier	$\Delta Q_{\mathbf{norm}}$ [Gt/km^2]	Retreat [km]	Mean gate depth [m]	Max gate depth [m]
91	Sverdrup	0.83 ± 0.20	6.2	-225 ± 164	-469
95	Kjer	0.97 ± 0.22	11.1	-228 ± 97	-345
113	Alison	0.55 ± 0.16	13.9	-99 ± 103	-218
134	Upernavik N	1.31 ± 0.33	6.6	- 27 ± 278	- 372
135	Upernavik C	0.51 ± 0.10	4.2	-167 ± 152	- 221

Upernavik C is attached to the same fjordal channel as Upernavik N. A clear pathway for BBIntW also exists towards Upernavik C's calving front (Figure 3.7b). Over the warming period, the change in normalised discharge (ΔQ_{norm}) added up to 0.51 ± 0.10 Gt/km^2. However, we detect that the initiation of discharge increase has a delay of about 10 years compared to the detected start of warming in 1997 (Figure 3.8b.3).

Over the complete period that we observe, Upernavik C retreated 4.2 km on a normal bed in a mostly parallel fjord. Around 2009 the fjord geometry changed to a widening state and modified to a parallel configuration in 2020. We find that the onset of discharge change roughly corresponds to the transformation of the fjord to a widening geometry (Figure 3.8b.3).

When we compare Upernavik N and Upernavik C, we find that the change in normalised discharge of the Upernavik N glacier is bigger than the Upernavik C glacier. We also detect that for Upernavik N, the period of warming corresponds to the period of changing discharge. For Upernavik C, the change in discharge is delayed compared to the warming period. The difference in magnitude and the delay of change of the Upernavik C glacier can be explained by the position of the calving front in time. Upernavik C has a more stable position, it retreated over a normal bed in a parallel fjord. Whilst Upernavik N retreated 5.9 km over an alternating normal and reverse bed in a widening fjord during a large part of the warming period (1998 - 2009) and only 0.7 km (2009 - 2020) when the fjord geometry changed to parallel retreat.

Upernavik S (136) shows very little retreat (0.6 km, Figure 3.7c) and decreasing discharge estimates (ΔQ_{norm} = -0.14 ± 0.02 Gt/km^2, Figure 3.8c.3). However, it is connected to the same fjordal channel as Upernavik N and Upernavik C, that do show large ΔQ_{norm}. We want to understand the difference between the neighbouring glaciers, therefore we decided to further investigate Upernavik S.

We identify that since 1989 Upernavik S had its calving front positioned on a sill (Figure 3.7c.2). The sill is high enough to block the inflow of BBIntW and therefore the BBIntW is assumed to not impact it. The glacier has been on a lateral pinning point until it moved over the sill before 2020. Since 2020 the glacier has started to retreat over a reverse bed from the lateral pinning point into a parallel fjord geometry.

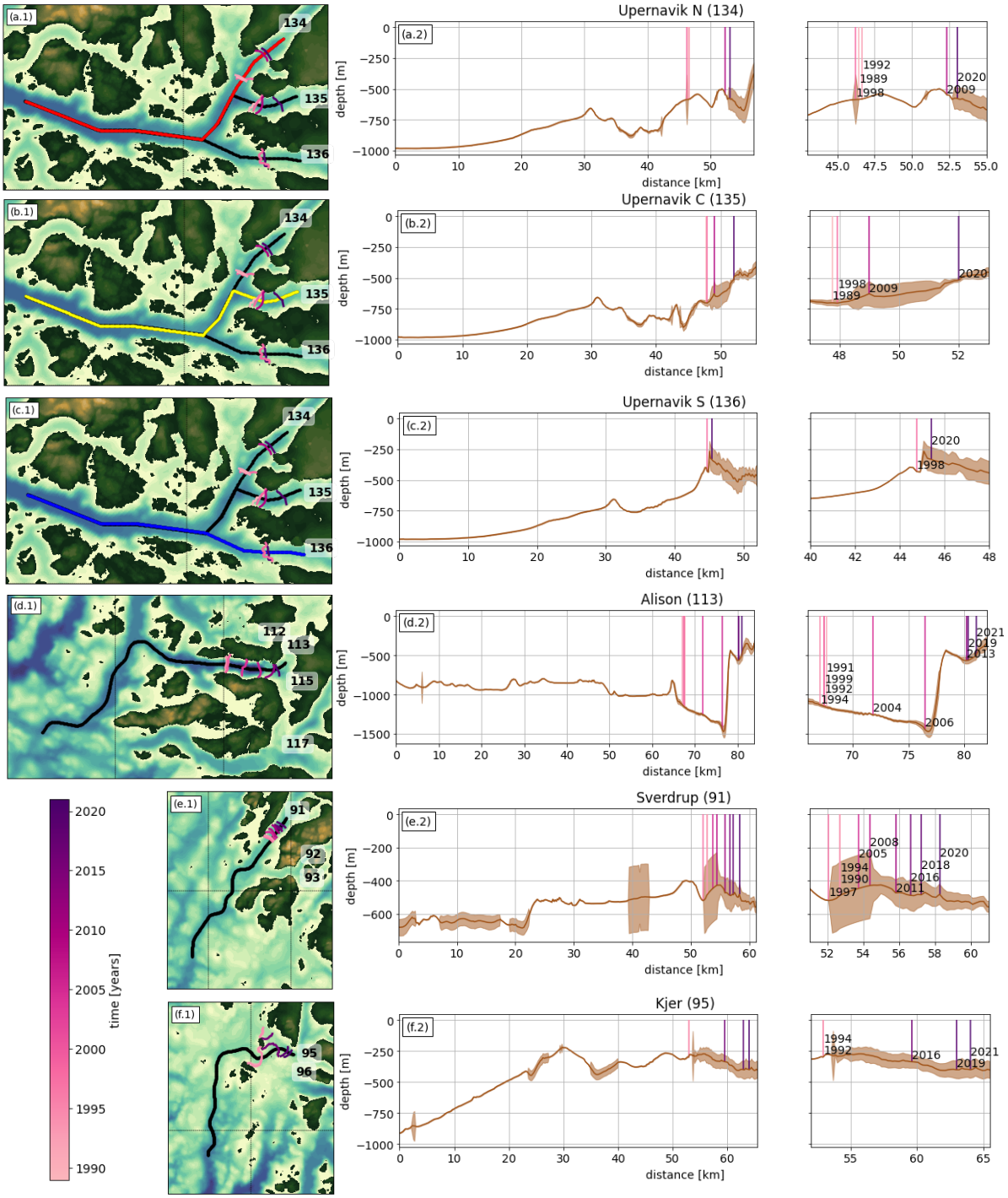

Figure 3.7: **Position of calving front on bed before, during and after warming period**. **(a)** Upernavik N (red), **(b)** Upernavik C (yellow), **(c)** Upernavik S (blue), **(d)** Alison, **(e)** Sverdrup, **(f)** Kjer. **(1)** Bathymetry from Bedmachine v4 and calving front positions. Lines indicate where the thalweg is positioned. **(2)** Thalwegs with historical calving front positions and zoom in on the historical calving fronts

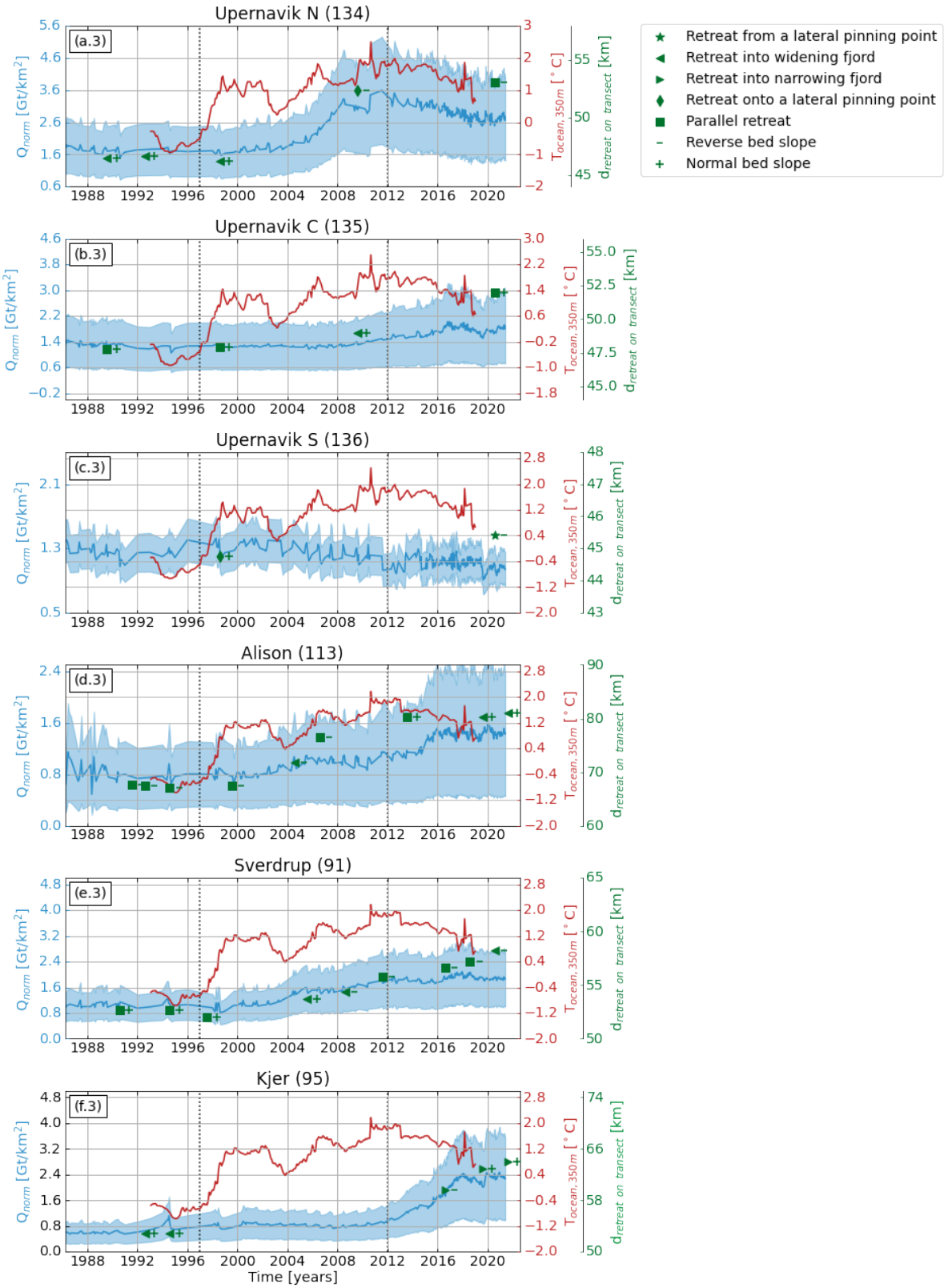

Figure 3.8: **Trends in normalised discharge estimates, temperature and retreat, changes in fjord geometry and bed slope over time**. **(a)** Upernavik N, **(b)** Upernavik C, **(c)** Upernavik S, **(d)** Alison, **(e)** Sverdrup, **(f)** Kjer. **(3)** Normalised discharge from 1986 - 2021 (blue, left axis), shaded area indicates the error of the normalised discharge estimate and HYCOM temperature from 1993 - 2018 at 350 m depth (red, right axis). In (a), (b) and (c) the temperature from location 8 (see Figure 3.4) is shown, as the Upernavik fjordal channel is connected to the Southern Canyon. In (d), (e) and (f) the temperature from location 10 is shown, as the Alison, Sverdrup and Kjer fjordal channels are connected to the Northern canyon. Vertical dotted lines indicate the observed warming period. Green markers indicate the fjord geometry at each calving front position in time. Type of bed slope at each calving front position is indicated by + (normal bed) and - (reverse bed).

Alison (113) has the deepest fjordal channel compared to the other glaciers, so there is a clear pathway for BBIntW (Figure 3.7d). In addition, we find that there are two periods of normalised discharge increase. The first between 2000 - 2005, which is during the warming period, the second from 2012 - 2016, which is during the slow cooling period of deep water of Atlantic origin (Figure 3.8d.3).

We detect that until 2006 Alison had retreated 9.4 km on a reverse bed since the warming started. From 2004, when the discharge trend stabilised, the shape changed from a parallel to a widening fjord. The glacier retreated 4.7 km in 2 years over this shape until 2006, when the fjord geometry became parallel again (Figure 3.8d.3). Even though the retreat was fast, and fjord geometry changed, the discharge estimates did not increase over this period. After 2006 we detect a sharp decrease in bed depth on which the glacier further retreated and found a more stable position. Since 2013 Alison has retreated only 0.6 km, while a second increase in the normalised discharge is observed.

Sverdrup (95) has a less pronounced and less wide fjordal channel compared to the other glaciers. However, the fjordal channel is still deep enough to be a pathway for Baffin Bay Intermediate Water (Figure 3.7e). Similar to Alison, in Sverdrup's discharge estimates, two periods can be distinguished (Figure 3.8e.3). The first increase started in 1998 and lasted until 2004, the second started in 2008 and ended in 2011. Both periods are within the warming period of the Atlantic Water.

The first increase in normalised discharge started when Sverdrup's retreat was on a normal bed with parallel geometry. We detect that the second increase in discharge started when the fjord geometry changed from a parallel to a widening shape and the bed slope evolved from normal to reverse. The glaciers has been retreating on a reverse bed since at least 2008. In addition, we detect that the retreat of Sverdrup does not show any sudden increases or decreases, it follows a linear trend.

Kjer (91) has a fjordal channel that blocks the path for Baffin Bay Intermediate Water (Figure 3.7f). The bed gradually decreases to a depth of 250 m well before the glacier calving front is reached. We also find that the normalised discharge only starts increasing when the slow cooling period of Baffin Bay Intermediate Water is reached in 2012 (Figure 3.8f.3). We therefore assume that the observed discharge change is due to a different process than ocean warming.

Kjer is the glacier that shows the largest retreat distance (11.1 km) after Alison. We identify that the retreat of the glacier initiated when the calving front was positioned on a normal bed in a widening fjord. During most part of the increase of normalised discharge, we find this configuration. From 2016 the discharge increase and retreat continued on a reverse bed into a narrowing fjord. The retreat distance was smaller after the normalised discharge trend stabilised from 2017.

4

Discussion

Synthesizing multiple data and model resources, we have found that the glaciers in Northwest Greenland are vulnerable to increases in normalised discharge due to warming of deep waters of Atlantic origin, due to changes in glacier geometry and due to the combination of both.

4.1. Pathways of Atlantic Water to the glaciers

The complex bathymetry in Northwest Greenland clearly controls the strength of the current and the steering of Baffin Bay Intermediate Water as they are transported northward along the shelfbreak in Baffin Bay. The canyons that incise the shelfbreak steer part of the flow into the Southern canyon. This branch advects warm BBItntW cyclonically around the canyon system. In addition, part of the flow that continues northward along the shelfbreak branches into the Northern canyon and circulates cyclonically. However, we identify that the more narrow topographically constraint Southern canyon induces much stronger inflow at depth into the canyon and stronger cyclonic circulation around the canyon compared to the much wider, less confined Northern canyon. The flow in Melville Bay is also impacted by the inner shelfbreak current that advects a branch of the warm BBIntW northward from the head of the Southern canyon, along the offshore edge of the fjordal network system (Figure 3.2b).

In addition to the important process of topographic steering, where flows follow contours of f/H, it is well known that canyons can impact cross-shelf exchange and introduce ageostrophic contributions to the dominant momentum balance, resulting in upwelling or downwelling of the Baffin Bay Intermediate Water (Allen and Durrieu De Madron 2009). In section 3.2 we have identified that topographic steering could steer the flows in Northwest Greenland, but the increase of the Rossby number (see definition in the Introduction, chapter 1) at both canyons can also initiate ageostrophic effects.

We hypothesize that the Baffin Bay Intermediate Water may be associated with upwelling within the canyons. Using the CTD data from September 2019, we detected BBIntW between 252 and 426 m in the Southern canyon and between 261 and 419 m in the Northern canyon (Figure 3.1), while Tang et al. (2004) found BBIntW in the interior of Baffin Bay between 300 and 800 m. This suggests that that BBIntW is positioned higher in the water column in the canyons compared to the interior of Baffin Bay.

However, the paper by Ramos-Musalem and Allen (2019) suggests that canyons are subjected to upwelling if the shelfbreak flow is from the North and downwelling if the shelfbreak flow is from the South. This implies that the northward current along the shelfbreak in Baffin Bay must result in downwelling canyons, while the CTD and FESOM model suggest that upwelling of warmer BBIntW occurs. The FESOM model is forced by realistic winds, and perhaps this is responsible for the upwelling in the canyons. This deserves further investigation and is beyond the scope of the current thesis.

As the Baffin Bay Intermediate Water circulates around the Southern canyon, the CTD data from September 2019 showed that the water on the Southern side of the Southern canyon was warmer than the water on the Northern side of the Southern canyon (Figure 3.3). Notably, the CTD profile on the South side (472), that coincides with the observed inflowing current, is persistently warmer than the other profiles over the full time period that the CTD data is available (2016 - 2020). This is consistent with the cyclonic circulation observed in the FESOM model within the Southern canyon and the loss of heat of the BBIntW as it circulates within the canyon system.

A similar cyclonic circulation is detected in the Northern canyon. However, the lack of contrast in BBIntW temperatures between the South and North side of the Northern canyon and the weaker flow displayed by the FESOM model indicate that the circulation is weaker, compared to the Southern canyon (Figure 3.2a). In the Northern canyon, the canyon length scale is much larger and the Rossby number is smaller compared to the Southern canyon, hence the ageostrophic effects would be weaker.

4.2. Vulnerability of glaciers to the Atlantic Water

Fjordal channels that are positioned in the South are assumed to be more vulnerable to changes in Atlantic Water than the North. When we compare the temperature of the inflowing BBIntW in both canyons in the CTD data from September 2019, we observe that the Southern canyon receives warmer water compared to the North. We therefore hypothesize that over the warming period the water in the Southern canyon reached higher temperatures than water in the Northern canyon.

Whether a glacier is vulnerable to the BBIntW also depends on the depth of the fjordal channel, since Atlantic Water is found at depth. We observe that 4 of the 5 glaciers (Upernavik N, Upernavik C, Alison and Sverdrup) that showed the highest normalised discharge change over the warming period are deep enough to be a pathway for Atlantic Water (Figure 3.7).

We identify that the final control on the vulnerability of the glacier to the Atlantic Water is the position of the fjord entrance along the canyon head. From the FESOM model we found that the fjordal channels that are connected to the South side of both canyons experience a direct inflow of BBIntW. Yet, we notice that the inflowing current in the Southern canyon is stronger than in the Northern canyon. The fjordal channels that are positioned more centrally or North along the canyon head are expected to experience a weaker inflow. However, the resolution of the FESOM model made it more difficult to identify an inflow at other locations than the South side of both canyons. In order to quantify this properly, a high resolution ocean model would be needed.

Nonetheless, we indeed observe that from the 5 glaciers showing the highest change in normalised discharge over the warming period, 3 (Upernavik N, Upernavik C and Alison) have their fjordal channel connected to the South side of a canyon. Upernavik N and Upernavik C are connected to the fjordal channel that experienced the strongest inflow of the warmest water over the warming period in Baffin Bay. Together they contributed 10% to the total normalised discharge change, of glaciers deeper than 100 m, that we observe in Northwest Greenland. Upernavik S is also connected to the Upernavik fjordal channel. However, this glacier showed a slight decrease in normalised discharge over the warming period. In contrast to Upernavik N and C, Upernavik S has its calving front positioned on a sill. Therefore, BBIntW cannot reach the calving front and as a consequence not impact it.

Alison is connected to the South side of the Northern canyon head and therefore also experiences a clear inflow of BBIntW. The glacier showed an increase of 0.55 Gt/km^2 (3% of total) in normalised discharge over the warming period. In addition, Alison experienced the largest retreat of 13.9 km. But the extensive retreat is partly due to the glacier losing its floating ice tongue between 2001 and 2005 (McFadden et al. 2011; Carr, Vieli, and Stokes 2013).

Sverdrup's fjordal channel has its entrance in the center of the Northern canyon. Compared to Alison's and Upernavik's fjordal channel entrance, a distinct inflow of BBIntW was not clearly distinguished from the FESOM model. Nonetheless, the fjordal channel is deep enough to be a clear pathway for BBIntW. In addition, we found that the period of changing discharge corresponds to the period of ocean warming. We therefore assume that the glacier is affected by warming of BBIntW at depth, which is in agreement with Wood et al. (2018). Here, a high resolution ocean model would allow to investigate if a clear inflow can be expected.

4.3. Role of glacier geometry on sensitivity to ocean forcing

The geometry of the glacier fjord at the calving front also impacts the vulnerability of a glacier to discharge change. For 4 of the 5 glaciers that showed the highest normalised discharge over the warming period, we detected that changes in fjord geometry corresponded to changes in normalised discharge. We especially found that normalised discharge increases over a widening fjord and stabilises when the geometry changes to a lateral pinning point or parallel retreat. The opposite is however detected for Alison, for this glacier the normalised discharge increases when the fjord geometry is parallel and stabilises when we observe a widening fjord. However, Alison had a floating ice tongue until 2001 - 2005, hence it is seen as an exception. Therefore, despite our observations at Alison, we still consider the change in width of the fjordal channel during the retreat of a glacier to be a big control on the trends observed in the normalised discharge estimates. Since we only investigated this correlation for 5 of the over 50 glaciers in Northwest Greenland, we suggest that it should be studied more extensively in future research, but is outside the scope of this thesis.

Contrasting to the geometry, we find that the bed slope is a less important control on the vulnerability of a glacier to changes in normalised discharge. We found that 4 of the 5 glaciers that showed highest normalised discharge change had their calving front positioned on a normal bed slope when the normalised discharge estimates started increasing. According to Bunce et al. (2018), higher retreat rates are more often associated with reverse bed slopes and lower retreat rates with normal bed slopes. However, we identify that the change in normalised discharge is not necessarily faster over a reverse bed compared to a normal bed. Again, we note that this result is based on 5 of the over 50 glaciers in Northwest Greenland and that it it deserves further investigation, but is outside the scope of this study.

4.4. Vulnerability to Atlantic Water and role of glacier geometry

When we combine the vulnerability of glaciers to warming of Atlantic Water and the role of glacier geometry on the sensitivity to ocean forcing, we identify that the increase of normalised discharge is initiated by ocean warming, but the normalised discharge is also controlled by the geometry of the glacier during its retreat.

We find the biggest change in normalised discharge at the glaciers that are connected to the Upernavik fjordal channel, that acted as the pathway for the warmest and strongest inflow of BBIntW. However, Upernavik N showed a discharge change over the warming period that was over twice as high compared to Upernavik C, even though temperature forcing was similar. Upernavik N retreated over a widening fjord during the ocean warming period, while Upernavik C was retreating in a parallel fjord. We consider the difference in fjord geometry to be the cause of the observed contrast. This highlights the control that fjord geometry has on the magnitude of normalised discharge change.

4.5. Vulnerability of glaciers due to other processes

While we did not investigate other processes, we found that other factors also contribute to the increase in discharge of a glacier and retreat of a glacier calving front. Changes in sea ice extent during winter periods can increase the calving rate of glaciers (Moon, Joughin, and Smith 2015). Also, atmospheric warming can result in surface thinning of glaciers (Csatho et al. 2014). However, these factors are not considered in this study.

4.6. Decadal timescales and the NAO

The detected ocean warming period in HYCOM (1997 - 2011) is 2 years longer than the period of NAO negative phase found by Rignot et al. (2012). In addition, the detected period is 4 years longer compared to the warming period of 1998 - 2007 found by Wood et al. (2021). As a result, glaciers were added into our analysis that showed discharge change due to other processes than ocean warming. Kjer, the glacier that showed the second highest discharge change over the warming period is one of them.

Kjer is the only glacier with high discharge change that has a blocked pathway for water of Atlantic origin. Also, the period of change in discharge does not correspond to the period of warming. Moon et al. (2020) relate the discharge change of Kjer to the reconfiguration of the Greenland Ice Sheet coastal margin. They found that the subtle velocity changes between 1985 and 2000 initiated a multidecadal pattern of change. The Southern outlet of Kjer sped up, while the Northern outlet slowed down. Subsequently, thinning of both outlets accelerated between 2007 and 2012. This period of acceleration corresponds to the period over which we first observe an increase in discharge. We also find that the calving fronts of the Southern and Northern outlet of Kjer merge into one calving front between 2016 and 2020, the period in which the discharge signal stabilises again.

5

Conclusion

This research aimed to identify to what extent the pathways of deep Atlantic Water (referred to as Baffin Bay Intermediate Water) increased the vulnerability of glaciers to changes in normalised discharge in Northwest Greenland over the observed ocean warming period. We have shown that these pathways of Baffin Bay Intermediate Water are crucial for understanding the vulnerability of certain glaciers to warm Atlantic Waters.

From the difference in temperature and circulation strength between the Southern and Northern canyon we found that glaciers positioned at lower latitudes are more vulnerable than glaciers positioned further North. In addition, since the inflow of Baffin Bay Intermediate Water is observed at the South side of both canyons, we identified that fjordal channels positioned at the South side of a canyon experience a stronger inflow and are therefore more vulnerable. Finally, a fjordal channel, leading to the glacier calving front, should be deep enough to be a pathway for Baffin Bay Intermediate Water, since the warm water is found at depth.

Five glaciers showed over 0.5 Gt/km^2 normalised discharge change over the observed warming period of Baffin Bay Intermediate Water (1997 - 2011). Three of those glaciers where connected to the South side of either of the canyons. The two glaciers (Upernavik N and Upernavik C) that were positioned on the South side of the Southern canyon, the most vulnerable position, made up 10% of the total normalised discharge change of marine terminating glaciers in Northwest Greenland.

We identified that Sverdrup, also in the top five of highest discharge change, was only vulnerable because of the depth of its fjordal channel. For this glacier the development of a high resolution ocean model would be beneficial to better understand why it showed such a substantial change.

When the period of normalised discharge change did not correspond to the period of ocean warming, either the glacier had a pathway for Baffin Bay Intermediate Water, but a stable fjord geometry delayed the onset of change (Upernavik C), or the glacier had a blocked pathway for Baffin Bay Intermediate Water (Kjer), and the difference is explained by the reconfiguration of the Greenland coastline due to extensive ice mass loss.

In addition, we detected that the vulnerability of a glacier to changes in normalised discharge also depends on the changes in fjord geometry during the retreat of the calving front. It is the combination of both the vulnerability to Atlantic Water and the sensitivity of the fjord geometry to ocean forcing that impacts the observed changes in normalised discharge. Other factors like sea ice extent and atmospheric conditions also contribute to changes but were outside the scope of this thesis.

6

Recommendations

To gain a more detailed understanding of both the pathways of Baffin Bay Intermediate Water in the fjordal channels and the correlation between fjord geometry changes and normalised discharge trends, we give three main recommendations considering both the ocean and the glacier perspective. We discuss the benefits of a parcel tracking study (section 6.1), we outline the possibilities when a high resolution ocean model is developed (section 6.2) and give advise on the needed next steps considering the study on the correlation between fjord geometry and normalised discharge (section 6.3).

6.1. Parcel tracking study

In the presented study, we derive the pathways of Atlantic Water by creating videos of the currents at depth over the time period of a month. A good approach to validate the observed circulation from the FESOM model in the canyons would be to carry out a parcel tracking study. In a parcel tracking study, the ocean model data and a start location are fed to a parcel tracking algorithm. This algorithm assesses the pathway of an ocean parcel from a specified starting point. Therefore, it also gives us the opportunity to investigate the travel time of the Atlantic Water from the Davis Strait to the canyons.

In addition, with a parcel tracking study, the circulation of the deep Atlantic Water in the canyons can be studied in more detail. It will increase our understanding of the impact that the topographic differences between the canyons have on the pathway of the observed ocean parcels. It can also indicate which part of the Baffin Bay Intermediate Water flows into the Southern or Northern canyon and which part continues with the shelfbreak current. At the head of both canyons we could identify which part moves with the inner shelfbreak current and which part circulates around the canyons.

6.2. Development of high resolution ocean model

The development of a high resolution ocean model provides many new opportunities, here we discuss three. From the FESOM model and the CTD data results we obtained that there is a difference in the circulation strength between the Southern and Northern canyon. Also, we observe upwelling in both canyons, even though downwelling is expected from theory (Ramos-Musalem and Allen 2019). A high resolution ocean model would allow us to assess the differences between the currents in both canyons in more detail and detect eddies that might form at the head, center or mouth of each canyon. In addition, we could examine the upwelling strength of both canyons.

The resolution of the FESOM model was too low to detect a clear inflow of BBIntW into the fjordal channel of Sverdrup. However, the glacier showed significantly high normalised discharge change over the warming period and its fjordal channel can be a pathway for BBIntW. Here, a high resolution ocean model will provide the opportunity to analyse the strength of the Atlantic Water inflow at depth at Sverdrup's fjordal channel entrance. In addition, we would be able to study the observed flows in every fjordal channel towards the calving fronts. The high resolution model can also provide in quantifying the melt potential at the calving fronts and increase our understanding of seasonal differences and mixing events.

Mixing events can occur under the impact of katabatic winds. Such strong downslope wind events are known to flush the upper layer within the fjord and in return strengthen the inflow of water at depth (Spall, Jackson, and Straneo 2017). It would therefore be beneficial to understand if such winds are common in Northwest Greenland and if so, the high resolution ocean model could facilitate our analysis on the exchange of warm Atlantic Waters between the canyons and the fjordal channels. A glacier that would be interesting to analyse during the occurence of such an event is Upernavik S. The glacier calving front is positioned at the end of the fjordal channel that receives the warmest water. Since the glacier recently moved over the sill in its fjord, BBIntW might impact the glacier during such strong inflow events as it might be able to pass the sill.

6.3. Correlation fjord geometry and discharge estimates

Our study indicates that the change in fjord geometry, and thus the change in width of a fjordal channel has control over the trends that we observe in the normalised discharge estimates. Further research should be done to quantify the possible correlation, as it can help in predicting the discharge changes under different temperature forcings of the BBIntW at depth. In order to do so, both the temporal resolution of the position of the calving fronts has to increase and the uncertainty in the normalised discharge estimates should decrease.

The temporal resolution of ice front positions can be increased by using SAR (Satellite Aperture Radar) data in addition to the spectral data sources. Data can be obtained from several different satellites including Sentinel-1, RADARSAT-1 and 2 and TerraSAR-X. The big benefit of SAR, an active satellite system, is its independence of sunlight and cloud cover, as the instrument sends out its own signal. Also, NASA's MEaSURE Ice Velocity and Ice Sheet Mapping project provided a database with calving fronts positions with annual resolution (Moon and Joughin 2008).

The normalised discharge estimates could be improved by considering the glacier elevations in time. Currently, we use two elevation datasets, GLISTIN and GIMP. The difference that we find in the normalised discharge estimates between the two is added as an extra uncertainty (subsection 2.3.1). Instead, we could use the GIMP 0715 surface elevations (Howat, Negrete, and Smith 2014) which are timestamped per pixel and adjust the surface in time using elevation changes from Khan et al. 2016. This way, we would essentially reverse the process which Mankoff et al. (2020) used to derive its discharge estimates and decrease the uncertainty in the normalised discharge estimates.

A

Overview glacier gates and names

Table A.1: Overview of glacier gate numbers and their corresponding name as defined by Mouginot et al. (2019)

gate	name
49	SAVISSUAQ_WWWW
54	YNGVAR_NIELSEN_BRAE
55	CARLOS
59	GADE-MORELL
62	DOCKER_SMITH_GLETSCHER_W
63	DOCKER_SMITH_GLETSCHER
67	ISSUUARSUIT_SERMIA
69	ISSUUARSUIT_SERMIA
71	ISSUUARSUIT_SERMIA
72	NONAME_NORTH_OSCAR
73	KONG_OSCAR_GLETSCHER
79	NANSEN_GLETSCHER
91	SVERDRUP_GLETSCHER
92	STEENSTRUP-DIETRICHSON
93	STEENSTRUP-DIETRICHSON
94	STEENSTRUP-DIETRICHSON
95	KJER_GLETSCHER
96	HAYES_GLETSCHER_N_NN
99	HAYES_GLETSCHER_N_NN
100	HAYES_GLETSCHER_N_NN
102	HAYES_GLETSCHER_N_NN
103	HAYES_GLETSCHER_N_NN
104	HAYES_GLETSCHER_M_SS
111	HAYES_GLETSCHER_M_SS
112	HAYES_GLETSCHER_M_SS
113	ALISON_GLETSCHER
115	ALISON_GLETSCHER
117	ILLULLIP_SERMIA

gate	name
118	CORNELL_GLETSCHER
119	CORNELL_GLETSCHER
122	USSING_BRAEER_N
125	USSING_BRAEER
126	USSING_BRAEER
127	QEQERTARSUUP_SERMIA
129	KAKIVFAAT_SERMIAT
132	NUNATAKASSAAP_SERMIA
133	UPERNAVIK_ISSTROM_N
134	UPERNAVIK_ISSTROM_N
135	UPERNAVIK_ISSTROM_C
136	UPERNAVIK_ISSTROM_S

B

Preprocessing of CTD data

In order to obtain potential temperature and potential density anomaly from the CTD data and classify the Baffin Bay Intermediate Water, the data had to be pre-processed. The conductivity and in-situ temperature measurements were used to calculate absolute salinity (SA), potential temperature (θ) and potential density anomaly (σ_θ). Conversions were done using the GSW Oceanographic toolbox package (Feistel 2008) for Python (IOC, SCOR, and IAPSO 2010).

First depth is converted to pressure by solving Equation B.1 for p using the function *p_from_z()* with inputs depth and latitude. The $\Psi - \Phi^0$ term was ignored. $\hat{h}^{75}\left(S_{\mathrm{SO}}, 0^{\circ}\mathrm{C}, p\right)$ is the 75-term expression for the specific enthalpy of Standard Seawater.

$$\hat{h}^{75}\left(S_{\mathrm{SO}}, 0^{\circ}\mathrm{C}, p\right) - \Psi - \Phi^0 + g(\phi, 0)\left(z - \frac{1}{2}\gamma z^2\right) = 0 \tag{B.1}$$

Conductivity measurements were used to obtain the practical salinity (SP) values using equations from UNESCO (1983). Input to the function *SP_from_C()* were conductivity, in-situ temperature and the obtained pressure from the previous step.

Then practical salinity was used to obtain absolute salinity, which is defined as the mass fraction of dissolved material in seawater (g/kg). The function *SA_from_SP()* was executed. It had the inputs practical salinity, pressure, longitude and latitude. The function follows the algorithm from McDougall et al. (2012) displayed in Figure B.1. The algorithm values are obtained from a look-up table.

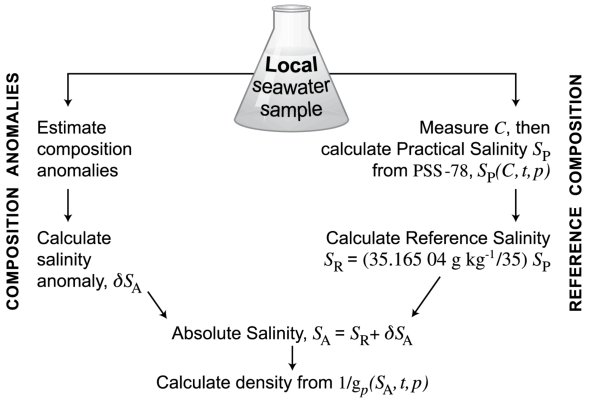

Figure B.1: Algorithm followed by *SA_from_SP()*. Figure from IOC, SCOR, and IAPSO (2010).

Potential temperature was calculated from absolute salinity, in-situ temperature and pressure using *pt0_from_t()*. The TEOS-10 algorithm uses an approach where the specific entropy of two seawater parcels is calculated. One before isentropic and isohaline pressure change, the other after, forming Equation B.2. Then potential temperature is found by iterating a modified Newton-Rhapson method twice (McDougall and Wotherspoon 2014). The reference pressure p_r is set to 0 dbar.

$$\eta(S_A, \theta, p, p_r) = \eta(S_A, t, p) \tag{B.2}$$

In order to calculate potential density anomaly, potential density had to be calculated first. IOC, SCOR, and IAPSO (2010) describes potential density as the density that a water parcel would have if pressure was changed to a fixed reference pressure in an isentropic and isohaline manner. The function *pot_rho_t_exact()* has the inputs absolute salinity, in-situ temperature pressure and reference pressure, which is again set to 0 dbar and is expressed in terms of the Gibbs function in Equation B.3.

$$\rho^{\theta}(S_A, t, p, p_r) = \rho\Big(S_A, \theta[S_A, t, p, p_r], p_r\Big) = g_P^{-1}\Big(S_A, \theta[S_A, t, p, p_r], p_r\Big) \tag{B.3}$$

Finally potential density anomaly was calculated using Equation B.4.

$$\sigma_\theta = \rho_\theta - 1000[kg/m^3] \tag{B.4}$$

C

Offset and bias in FESOM model

We detected both an offset and bias in the potential temperature and practical salinity results of the FESOM model. In this appendix the FESOM model results are compared to CTD data from corresponding dates. Both the Southern and Northern canyon sections were analysed for the year 2019. For the Northern canyon a section containing CTD profiles 455, 457, 459 and 461 is obtained. The profiles were collected on the 4th of September 2019. CTD profiles 468, 469 and 472 form the section for the Southern canyon and were obtained on the 30th of August 2019. Figure C.1 shows the location of the CTD profiles.

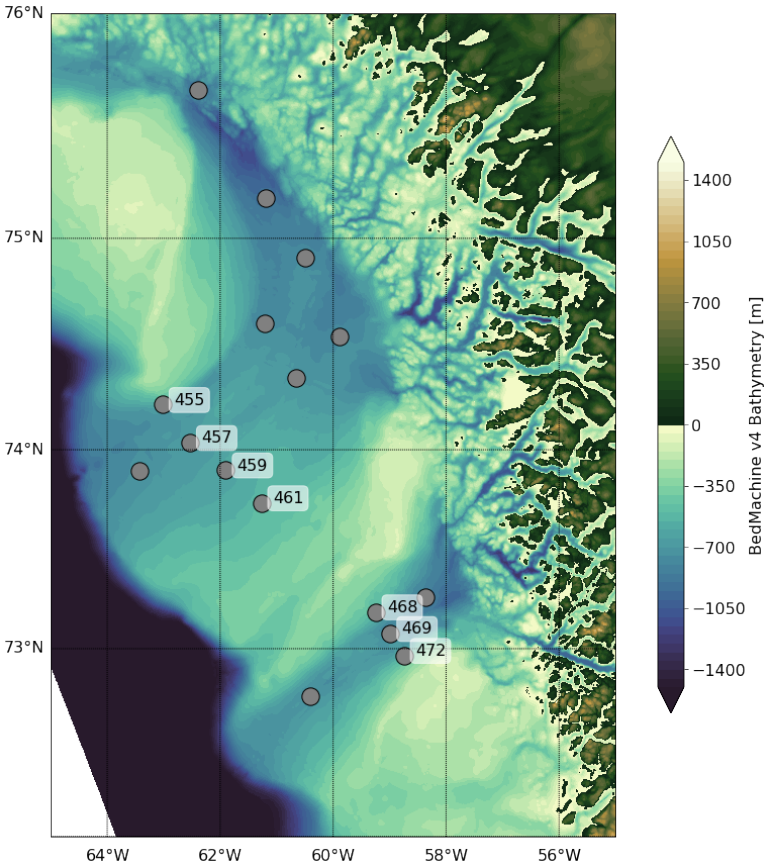

Figure C.1: **Location of sections in Southern and Northern canyon**. Northern canyon section consists of CTD profile 455, 457, 459 and 461. Southern canyon section consists of CTD profile 468, 469, 472. FESOM sections are taken from 455 to 461 and 468 to 472

The potential temperature sections in Figure C.2 and Figure C.3 indicate that there is a bias in the warm layer (yellow) of the FESOM model of at least +2.5°C. Note that the colorbar of the CTD and FESOM cross section is different, otherwise the gradient in the FESOM data was not apparent. In addition, the depth of warmer water was estimated to be more shallow. In the Southern canyon, the warmest water was found from 300 m depth, while in the FESOM model, the warmest water appeared from 200 m. In the Northern canyon, the warmest water was detected at 400 m, while in FESOM the maximum temperatures were found at 300 m. Finally, it was observed that the FESOM model estimated a significantly larger temperature gradient between the temperature of the warmest layer and the layer at depth. In the model the temperature decreased from 5.0°C to 1.0°C over depth, while in the CTD's we observed a temperature gradient between 2.5°C at 300 m and about 1.0°C at depth (> 600 m). In the Northern canyon we found the same patterns in temperature differences between the warmest layer and the layer at depth.

Similar to potential temperature, the practical salinity of the FESOM model also showed a bias and offset. We found that the FESOM model results showed higher practical salinity at depth compared to the CTD's in both the Southern and the Northern canyon. However, more pronounced was the difference in gradient. It is known from Figure C.2, Figure C.3 and Tang et al. (2004) and Gladish, Holland, and Lee (2015) that salinity only increases down to deeper depths. Contrastingly, FESOM showed a decrease in salinity from 400 m up to the ocean floor.

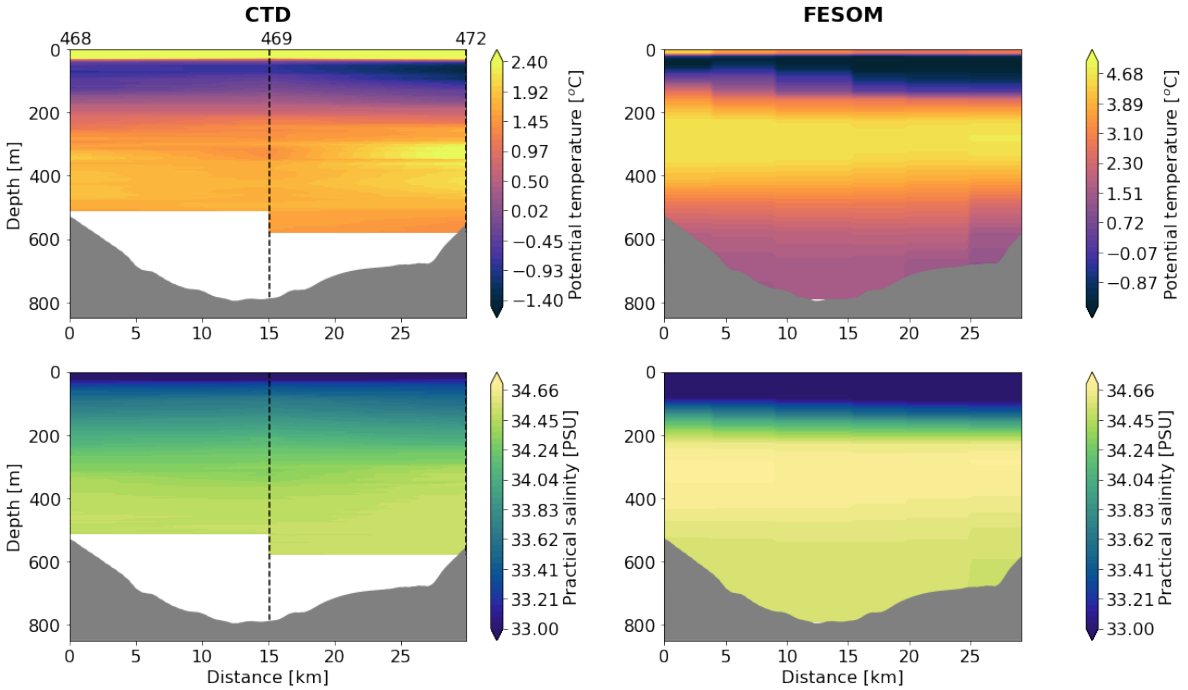

Figure C.2: **CTD and FESOM potential temperature and practical salinity results for the Southern canyon**. CTD profiles 468, 469 and 471 are from 30/08/2019. The FESOM profile is taken from the location of probe 468 to the location of probe 472 for 30/08/2019. Grey shaded area is the bottom topography. **(Top)**: Potential temperature for CTD (left) and FESOM (right). Note that the range of the colorbar is different for both plots, for CTD $-1.5 < \theta < 2.5$°C and for FESOM $-1.5 < \theta < 5.0$°C. **(Bottom)**: Salinity for CTD (left) and FESOM (right). Note that the salinity is in PSU, since FESOM model salinity is practical salinity instead of absolute salinity.

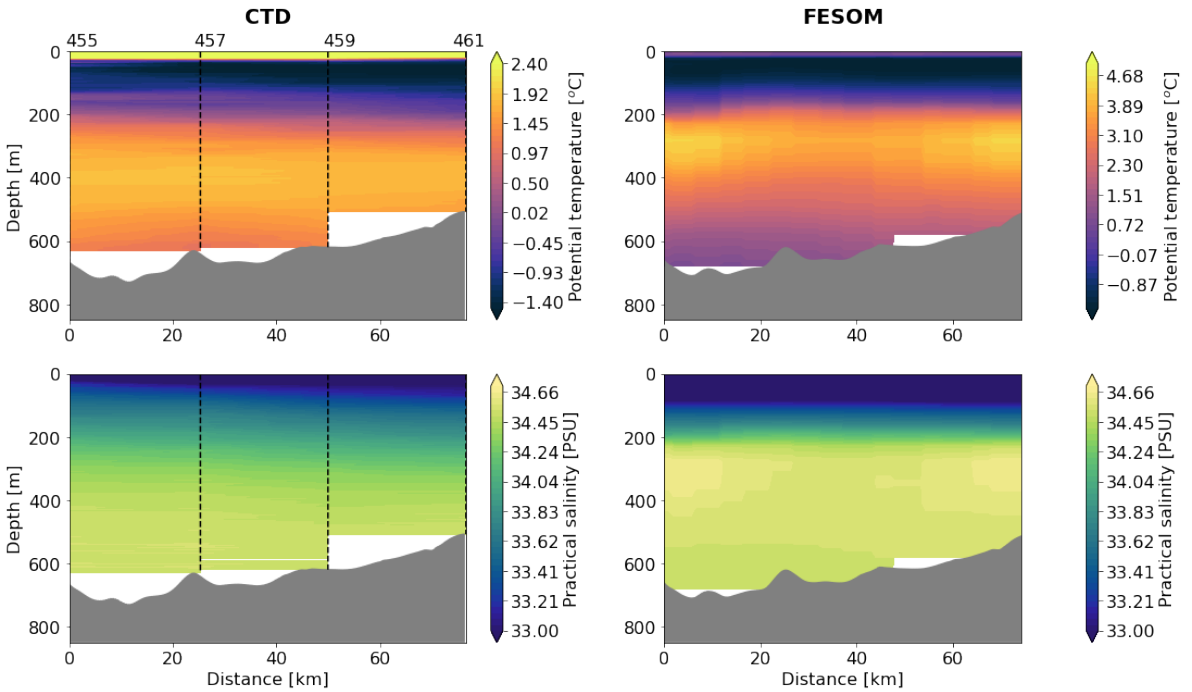

Figure C.3: **CTD and FESOM potential temperature and practical salinity results for the Northern canyon**. CTD profiles 455, 457, 459 and 461 are from 04/09/2019. The FESOM profile is taken from the location of probe 455 to the location of probe 461 for 04/09/2019. Grey shaded area is the bottom topography. **(Top)**: Potential temperature for CTD (left) and FESOM (right). Note that the range of the colorbar is different for both plots, for CTD $-1.5 < \theta < 2.5$°C and for FESOM $-1.5 < \theta < 5.0$°C. **(Bottom)**: Salinity for CTD (left) and FESOM (right). Note that the salinity is in PSU, since FESOM model salinity is practical salinity instead of absolute salinity.

Even though we found a bias and offset between the CTD data and FESOM model results, the model still clearly indicates the correct order of water masses. From warmer surface layers, to the colder Baffin Bay Thermal Water which is found on top of the warm Baffin Bay Intermediate Water. Also, the FESOM model was only used to determine the pathways of Atlantic Water in space and the flow that is displayed by the model was realistic. Therefore, the bias and offset do not pose a problem.

D

Southern canyon cross sections 2016 - 2020

This appendix shows the CTD sections in the Southern canyon highlighting the persistence of the warmer Atlantic originating water at the South side of the canyon for 2016, 2017 and 2020. CTD profiles 468, 469, 472 were not obtained in 2018, therefore that year is not displayed.

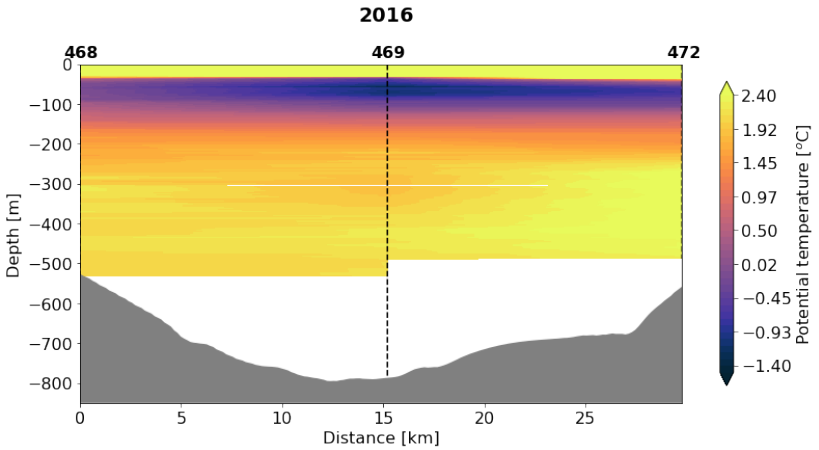

Figure D.1: **CTD section Southern canyon in 2016**. CTD cross section for the Southern canyon of CTD probes 468, 469, 472 obtained on 24-09-2016

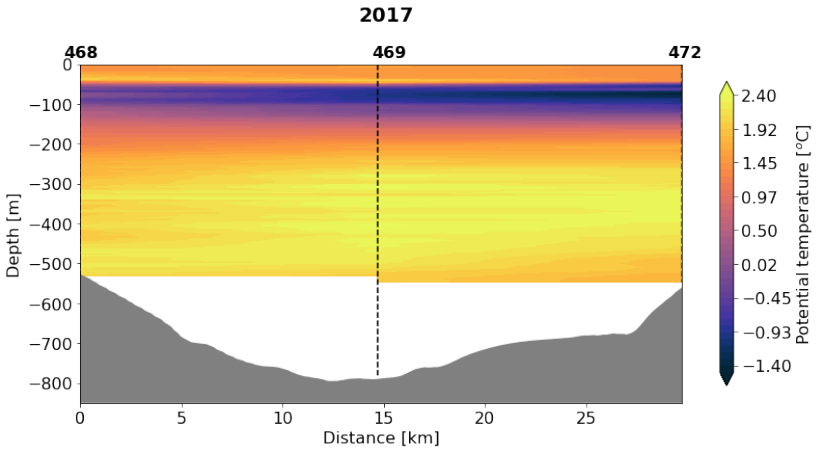

Figure D.2: **CTD section Southern canyon in 2017**. CTD cross section for the Southern canyon of CTD probes 468, 469, 472 obtained on 19-10-2017

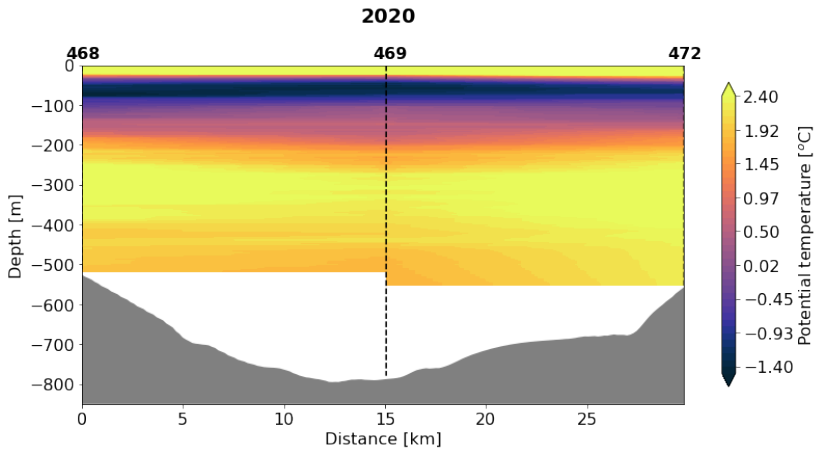

Figure D.3: **CTD section Southern canyon in 2020**. CTD cross section for the Southern canyon of CTD probes 468, 469, 472 obtained on 26-08-2020

Bibliography

Allen, S E, and X Durrieu De Madron. 2009. “A review of the role of submarine canyons in deep-ocean exchange with the shelf.” *Ocean Sci* 5:607–620. www.ocean-sci.net/5/607/2009/.

An, Lu, Eric Rignot, Romain Millan, Kirsty Tinto, and Josh Willis. 2019. “Bathymetry of Northwest Greenland using "Ocean Melting Greenland" (OMG) high-resolution airborne gravity and other data.” *Remote Sensing,* ISSN: 20724292. https://doi.org/10.3390/rs11020131.

Bindoff, N. L., P. A. Stott, K. M. AchutaRao, M. R. Allen, N. Gillett, D. Gutzler, K. Hansingo, et al. 2013. “Detection and attribution of climate change: From global to regional.” In *Climate Change 2013: The Physical Science Basis. Contribution of Working Group I to the Fifth Assessment Report of the Intergovernmental Panel on Climate Change,* edited by T. F. Stocker, D. Qin, G.-K. Plattner, M. Tignor, S. K. Allen, J. Doschung, A. Nauels, Y. Xia, V. Bex, and P. M. Midgley, 867–952. Cambridge, UK: Cambridge University Press. https://doi.org/10.1017/CBO9781107415324.022.

Bindoff, Nathaniel L, William WL Cheung, James Gitundu Kairo, Javier Arıstegui, Valeria Ana Guinder, Robert Hallberg, Nathalie Jeanne Marie Hilmi, Nianzhi Jiao, Md Saiful Karim, Lisa Levin, et al. 2019. “Changing ocean, marine ecosystems, and dependent communities.” *IPCC special report on the ocean and cryosphere in a changing climate,* 477–587.

Bunce, Charlie, J. Rachel Carr, Peter W. Nienow, Neil Ross, and Rebecca Killick. 2018. “Ice front change of marine-terminating outlet glaciers in northwest and southeast Greenland during the 21st century.” *Journal of Glaciology,* ISSN: 00221430. https://doi.org/10.1017/jog.2018.44.

Carr, J Rachel, Chris Stokes, and Andreas Vieli. 2014. “Recent retreat of major outlet glaciers on Novaya Zemlya, Russian Arctic, influenced by fjord geometry and sea-ice conditions.” *Journal of Glaciology* 60 (219): 155–170.

Carr, J. Rachel, Andreas Vieli, and Chris Stokes. 2013. “Influence of sea ice decline, atmospheric warming, and glacier width on marine-terminating outlet glacier behavior in northwest Greenland at seasonal to interannual timescales.” *Journal of Geophysical Research: Earth Surface* 118 (3): 1210–1226. ISSN: 21699011. https://doi.org/10.1002/jgrf.20088.

Chassignet, Eric P, Harley E Hurlburt, Ole Martin Smedstad, George R Halliwell, Patrick J Hogan, Alan J Wallcraft, Remy Baraille, and Rainer Bleck. 2007. “The HYCOM (hybrid coordinate ocean model) data assimilative system.” *Journal of Marine Systems* 65 (1-4): 60–83.

Csatho, Beata M, Anton F Schenk, Cornelis J van der Veen, Gregory Babonis, Kyle Duncan, Soroush Rezvanbehbahani, Michiel R Van Den Broeke, Sebastian B Simonsen, Sudhagar Nagarajan, and Jan H Van Angelen. 2014. “Laser altimetry reveals complex pattern of Greenland Ice Sheet dynamics.” *Proceedings of the National Academy of Sciences* 111 (52): 18478–18483.

Cuny, Jérôme, Peter B Rhines, and Ron Kwok. 2005. “Davis Strait volume, freshwater and heat fluxes.” *Deep Sea Research Part I: Oceanographic Research Papers* 52 (3): 519–542.

Curry, B, CM Lee, B Petrie, RE Moritz, and R Kwok. 2014. “Multiyear volume, liquid freshwater, and sea ice transports through Davis Strait, 2004–10.” *Journal of Physical Oceanography* 44 (4): 1244–1266.

Feistel, Rainer. 2008. "A Gibbs function for seawater thermodynamics for -6 to 80 °C and salinity up to 120 g kg-1." *Deep-Sea Research Part I: Oceanographic Research Papers* 55 (12): 1639–1671. ISSN: 09670637. https://doi.org/10.1016/j.dsr.2008.07.004.

Fenty, Ian, Josh K. Willis, Ala Khazendar, Steven Dinardo, René Forsberg, Ichiro Fukumori, David Holland, et al. 2016. "Oceans melting Greenland: Early results from NASA's ocean-ice mission in Greenland." *Oceanography,* ISSN: 10428275. https://doi.org/10.5670/oceanog.2016.100.

Gladish, Carl V, David M Holland, and Craig M Lee. 2015. "Oceanic Boundary Conditions for Jakobshavn Glacier. Part II: Provenance and Sources of Variability of Disko Bay and Ilulissat Icefjord Waters, 1990-2011*." *Journal of Physical Oceanography* 45:33–66. https://doi.org/10.1175/JPO-D-14. http://dx.doi.org/10.1175/JPO-D-14-.

Grivault, Nathan, Xianmin Hu, and Paul G. Myers. 2017. "Evolution of Baffin Bay Water Masses and Transports in a Numerical Sensitivity Experiment under Enhanced Greenland Melt." *Atmosphere - Ocean* 55, no. 3 (May): 169–194. ISSN: 14809214. https://doi.org/10.1080/07055900.2017.1333950.

Howat, I.M., A. Negrete, and B.E. Smith. 2014. "The Greenland Ice Mapping Project (GIMP) land classification and surface elevation datasets." *The Cryosphere* 8:1509–1518. https://doi.org/10.5194/tc-8-1509-2014.

IOC, SCOR, and IAPSO. 2010. "The international thermodynamic equation of seawater-2010: Calculation and use of thermodynamic properties." *Intergovernmental Oceanographic Commision, Manuals and Guides No. 56, UNESCO.*

Khan, Shfaqat A, Ingo Sasgen, Michael Bevis, Tonie van Dam, Jonathan L Bamber, John Wahr, Michael Willis, Kurt H Kjær, Bert Wouters, Veit Helm, et al. 2016. "Geodetic measurements reveal similarities between post–Last Glacial Maximum and present-day mass loss from the Greenland ice sheet." *Science advances* 2 (9): e1600931.

Khazendar, Ala, Ian G. Fenty, Dustin Carroll, Alex Gardner, Craig M. Lee, Ichiro Fukumori, Ou Wang, et al. 2019. "Interruption of two decades of Jakobshavn Isbrae acceleration and thinning as regional ocean cools." *Nature Geoscience,* ISSN: 17520908. https://doi.org/10.1038/s41561-019-0329-3.

King, Michalea D, Ian M Howat, Salvatore G Candela, Myoung J Noh, Seongsu Jeong, Brice P Y Noël, Michiel R van den Broeke, Bert Wouters, and Adelaide Negrete. 2020. "Dynamic ice loss from the Greenland Ice Sheet driven by sustained glacier retreat." *Communications Earth Environment* 1 (1): 1. ISSN: 2662-4435. https://doi.org/10.1038/s43247-020-0001-2. https://doi.org/10.1038/s43247-020-0001-2.

Mankoff, K. D., A. Solgaard, W. Colgan, A. P. Ahlstrøm, S. A. Khan, and R. S. Fausto. 2020. "Greenland Ice Sheet solid ice discharge from 1986 through March 2020." *Earth System Science Data* 12 (2): 1367–1383. https://doi.org/10.5194/essd-12-1367-2020. https://essd.copernicus.org/articles/12/1367/2020/.

McDougall, T. J., D. R. Jackett, F. J. Millero, R. Pawlowicz, and P. M. Barker. 2012. "A global algorithm for estimating Absolute Salinity." *Ocean Science* 8 (6): 1123–1134. https://doi.org/10.5194/os-8-1123-2012. https://os.copernicus.org/articles/8/1123/2012/.

McDougall, Trevor J., and Simon J. Wotherspoon. 2014. "A simple modification of Newton's method to achieve convergence of order 1 + 2." *Applied Mathematics Letters* 29 (March): 20–25. ISSN: 08939659. https://doi.org/10.1016/j.aml.2013.10.008.

McFadden, Ellyn M, Ian M Howat, Ian Joughin, Ben E Smith, and Yushin Ahn. 2011. "Changes in the dynamics of marine terminating outlet glaciers in west Greenland (2000–2009)." *Journal of Geophysical Research: Earth Surface* 116 (F2).

Moon, Twila, and Ian Joughin. 2008. "Changes in ice front position on Greenland's outlet glaciers from 1992 to 2007." *Journal of Geophysical Research: Earth Surface* 113 (F2).

Moon, Twila, Ian Joughin, and Ben Smith. 2015. "Seasonal to multiyear variability of glacier surface velocity, terminus position, and sea ice/ice mélange in northwest Greenland." *Journal of Geophysical Research: Earth Surface* 120 (5): 818–833.

Moon, Twila A., Alex S. Gardner, Beata Csatho, Ivan Parmuzin, and Mark A. Fahnestock. 2020. "Rapid Reconfiguration of the Greenland Ice Sheet Coastal Margin." *Journal of Geophysical Research: Earth Surface* 125 (11). ISSN: 21699011. https://doi.org/10.1029/2020JF005585.

Morlighem, M. 2021. *IceBridge BedMachine Greenland, Version 4*. https://doi.org/10.5067/VLJ5YXKCNGXO.

Morlighem, M., C. N. Williams, E. Rignot, L. An, J. E. Arndt, J. L. Bamber, G. Catania, et al. 2017. "BedMachine v3: Complete Bed Topography and Ocean Bathymetry Mapping of Greenland From Multibeam Echo Sounding Combined With Mass Conservation." *Geophysical Research Letters,* ISSN: 19448007. https://doi.org/10.1002/2017GL074954.

Mouginot, Jérémie, Eric Rignot, Anders A. Bjørk, Michiel van den Broeke, Romain Millan, Mathieu Morlighem, Brice Noël, Bernd Scheuchl, and Michael Wood. 2019. *Forty-six years of Greenland Ice Sheet mass balance from 1972 to 2018*. https://doi.org/10.1073/pnas.1904242116.

Münchow, Andreas, Janin Schaffer, and Torsten Kanzow. 2020. "Ocean circulation connecting Fram Strait to glaciers off northeast Greenland: Mean flows, topographic Rossby waves, and their Forcing." *Journal of Physical Oceanography* 50 (2): 509–530.

Murray, T., K. Scharrer, N. Selmes, A. D. Booth, T. D. James, S. L. Bevan, J. Bradley, et al. 2015. "Extensive retreat of Greenland tidewater glaciers, 2000–2010." *Arctic, Antarctic, and Alpine Research* 47 (3): 427–447. https://doi.org/10.1657/AAAR0014-049. eprint: https://doi.org/10.1657/AAAR0014-049. https://doi.org/10.1657/AAAR0014-049.

Myers, Paul G, Chris Donnelly, and Mads H Ribergaard. 2009. "Structure and variability of the West Greenland Current in summer derived from 6 repeat standard sections." *Progress in Oceanography* 80 (1-2): 93–112.

OMG Mission. 2020a. *Glacier elevation data from the GLISTIN-A campaigns. Ver. 1. PO.DAAC, CA, USA. Dataset accessed 2021-09-28*. https://dx.doi.org/10.5067/OMGEV-GLNA1.

OMG Mission. 2020b. *OMG Airborne eXpendable Conductivity Temperature Depth (AXCTD) Profiles. Ver. 1. PO.DAAC, CA, USA. Dataset accessed 2021-04-13*. https://dx.doi.org/10.5067/OMGEV-GLNA1.

Ramos-Musalem, Karina, and Susan E. Allen. 2019. "The impact of locally enhanced vertical diffusivity on the cross-shelf transport of tracers induced by a submarine canyon." *Journal of Physical Oceanography* 49 (2). ISSN: 15200485. https://doi.org/10.1175/JPO-D-18-0174.1.

Rignot, E, I Fenty, D Menemenlis, and Y Xu. 2012. "Spreading of warm ocean waters around Greenland as a possible cause for glacier acceleration." *Annals of Glaciology* 53 (60): 257–266.

Rignot, E., I. Fenty, Y. Xu, C. Cai, and C. Kemp. 2015. "Undercutting of marine-terminating glaciers in West Greenland." *Geophysical Research Letters,* ISSN: 19448007. https://doi.org/10.1002/2015GL064236.

Rudels, Bert, Eberhard Fahrbach, Jens Meincke, Gereon Budéus, and Patrick Eriksson. 2002. "The East Greenland Current and its contribution to the Denmark Strait overflow." *ICES Journal of Marine Science* 59 (6): 1133–1154.

Sarafanov, Artem. 2009. "On the effect of the North Atlantic Oscillation on temperature and salinity of the subpolar North Atlantic intermediate and deep waters." *ICES Journal of Marine Science* 66 (7): 1448–1454.

Spall, Michael A., Rebecca H. Jackson, and Fiammetta Straneo. 2017. "Katabatic Wind-Driven Exchange in Fjords." *Journal of Geophysical Research: Oceans* 122 (10): 8246–8262. ISSN: 21699291. https://doi.org/10.1002/2017JC013026.

Tang, Charles C.L., Charles K. Ross, Tom Yao, Brian Petrie, Brendan M. DeTracey, and Ewa Dunlap. 2004. *The circulation, water masses and sea-ice of Baffin Bay,* 4. https://doi.org/10.1016/j.pocean.2004.09.005.

UNESCO. 1983. "Algorithms for computation of fundamental properties of seawater." *Unesco technical papers in marine science*.

Wood, M., E. Rignot, I. Fenty, D. Menemenlis, R. Millan, M. Morlighem, J. Mouginot, and H. Seroussi. 2018. "Ocean-Induced Melt Triggers Glacier Retreat in Northwest Greenland." *Geophysical Research Letters* 45 (16). ISSN: 19448007. https://doi.org/10.1029/2018GL078024.

Wood, M., Eric Rignot, Ian Fenty, Lu An, Anders Bjørk, Michiel van den Broeke, Cilan Cai, et al. 2021. "Ocean forcing drives glacier retreat in Greenland." *Science Advances* 7 (1). ISSN: 23752548. https://doi.org/10.1126/sciadv.aba7282.